Exploitation of the Mesosphere (MesosphEO)

ESA MesosphEO

Literature Survey Document (LSD)

ITT ESA/AO/1-7759/14/SB-NC

Date: 23-03-2015

Version: LSD 1.2

WP Manager:
M. Rapp, M. Dameris and B. Kaifler

WP Manager Organisation:
DLR

DOCUMENT CHANGE RECORD

Issue	Revision	Date	Modified items
1	0	30/01/2015	First draft of the document
1	1	11/03/2015	Minor revision
1	2	23/03/2015	Minor revision

Table of Contents

1 Introduction

The purpose of the Literature Survey Document in the MesosphEO project is to give an overview of available satellite data products and models applicable to the mesosphere.

The history of satellite-based atmospheric measurements dates back to the 1970s. During the last four decades, several satellite missions with instrumentation dedicated for atmospheric research were launched. Missions which are most relevant for the MesosphEO project are listed in Table 1 for reference. Among the main quantities retrieved from satellite observations are atmospheric temperature, ozone, water vapour, methane, carbon oxides (CO and CO_2) and nitrogen oxides. Particular interest was given to mesospheric aerosol layers known as polar mesospheric clouds (PMCs, also known as noctilucent clouds, NLCs) that consist of ice particles and whose sensitivity to climate change was debated. Data products retrieved form satellite observations which are important for the MesosphEO project are listed in section 2.

In section 3 we provide an overview of general circulation models, often coupled to chemistry models, which are suitable for mesospheric studies. Physical processes are implemented in the models to various degrees, and the top altitudes of the models vary considerably. This makes certain models suitable for specific types of studies.

Insights gained by mesospheric observations and the current understanding of physical processes relevant to the mesosphere are reviewed in section 4. In the last decade, extensive comparisons between model runs and observations were undertaken. The quest to improve models to match atmospheric observations has greatly benefitted the understanding of e.g. dynamical processes relevant to the mesosphere.

Section 5 concludes with open questions and key points for future work.

Satellite	Instrument	Operation
ENVISAT (Environmental Satellite)	MIPAS (Michelson Interferometer for Passive Atmospheric Sounding) SCIAMACHY (Scanning Imaging Absorption SpectroMeter for Atmospheric CHartography) GOMOS (Global Ozone Monitoring by Occultation of Stars)	03/2002 - 04/2012
Odin	OSIRIS (Optical Spectrograph and InfraRed Imager System) SMR (Sub-Millimetre Radiometer)	02/2001 - ongoing
TIMED (Thermosphere Ionosphere Mesosphere Energetics and Dynamics)	SABER (Sounding of the Atmosphere using Broadband Emission Radiometry)	12/2001 - ongoing
SCISAT-1	ACE-FTS (Atmospheric Chemistry Experiment – Fourier Transform Spectrometer)	02/2004 - ongoing
Aura	MLS (Microwave Limb Sounder)	07/2004 - ongoing
AIM (Aeronomy of Ice in the Mesosphere)	SOFIE (Solar Occultation for Ice Experiment) CIPS (Cloud Imaging and Particle Size Experiment)	04/2007 - ongoing
UARS (Upper Atmosphere Research Satellite)	HALOE (Halogen Occultation Experiment) WINDII (Wind Imaging Interferometer)	09/1991 - 12/2005
NOAA weather satellites (series)	SBUV series (Solar Backscatter Ultraviolet Radiometer)	1984 - ongoing
ERBS (Earth Radiation Budget Satellite)	SAGE II (Stratospheric Aerosol and Gas Experiment)	10/1984 - 10/2005

Table 1. Main satellites and instruments relevant for MesosphEO.

2 Available measurement data

Satellite-based measurements are advantageous for global studies, but they bear some shortcomings. It takes a full day to describe a planetary-scale pattern; a given point on Earth is observed only once every several days at a given time of day. This may introduce spurious tidal effects in long-term trend detection. Moreover, incomplete (limited) satellite data sampling leads to concerns relating to data aliasing and spatial/temporal ambiguities. Satellite measurements are subject to drift due to aging and exposure to charged particle fluxes in space. However, considerable efforts are made to estimate the effects of these problems using internal proxies. Also, unless the orbit is Sun-synchronous, the local solar time of the measurement will periodically change for each location. Another limitation of these measurements is their relatively limited temporal extension, until now (Beig et al., 2003).

In the following we review observations of atmospheric temperature, ozone, water vapour, methane, carbon oxides, nitrogen oxides, and PMC.

2.1 Temperature observations

A good dataset of temperature and chemical species (see below) is derived from **MIPAS** measurements in an altitude range between 20 km to 105 km, from 2005 to 2012; information is available as well for PMCs. MIPAS temperature observations are available with a vertical resolution of 4-6 km at 50-90 km and 6-10 km above, and 300-500 km horizontal resolution along track (von Clarmann et al., 2009, García-Comas et al., 2012). Comparison of vM21 MIPAS temperatures with ACE-FTS, MLS, OSIRIS, SABER, SOFIE and lidar measurements yield differences smaller than 2 K at 50-80 km except for summer at high latitudes, where the difference is smaller than 5 K at 65-80 km (García-Comas et al., 2012, 2014). The vertical resolution of temperature and NO profiles at high latitudes ranges between 5-10 km and 10-20 km depending on magnetic activity (Bermejo-Pantaleón, 2011).

Recently, a new product of mesospheric temperatures was derived from observations with **OSIRIS**. Temperature profiles are retrieved between 45 km and 105 km. The accuracy is better than 6 K near 105 km, better than 3 K at 90 km, and better than 8 K at 85 km (Sheese et al., 2012). Coverage is nearly global, 82°N-82°S.

Temperature profiles retrieved from observations with **SABER** are available between 10 km and 110 km. The coverage in south-viewing mode is between 83°S and 52°N and in north-viewing mode between 83°N and 52°N with a repeat cycle of 60 days. Observations with the SABER instrument started in January 2002 (Remsberg et al., 2008).

The **ACE-FTS** instrument began observing the atmosphere routinely in February 2004. ACE-FTS temperature profiles are available between 12 km and 115 km altitude (Sica et al., 2008; Boone et al., 2005; Boone et al., 2013). The vertical resolution is 3-4 km with vertical spacing of measurements ranging from 2-6 km in the mesosphere.

Data from **Aura MLS** is available since 2004. The vertical resolution of the temperature profiles is 3 km at 31.6 hPa and about 13 km at 0.001 hPa. Temperature precision is 1 K or better from 316 hPa to 3.16 hPa, and about 3 K at 0.001 hPa (Schwartz et al., 2008).

Nearly continuous temperature data at high latitudes between 65° and 85° are available from **SOFIE** since May 2007 (Russell et al., 2009; Gordley et al., 2009). The version 1.2 temperature data product has an altitude range of 15-95 km with a vertical resolution ranging between 1 km and 2 km (Liu et al., 2014).

Mesospheric temperature measurements from eight years of observations from **SMR** are analyzed by Orsolini et al. (2010).

2.2 Observation of ozone

Measurements with **MIPAS** has provided a very good quality dataset of middle atmospheric O_3 (incl. water vapour, NO and NO_2) up to 100 km, yet with limited temporal coverage (2005-2012). Examples are given in Figure 1, showing observations during day and night.

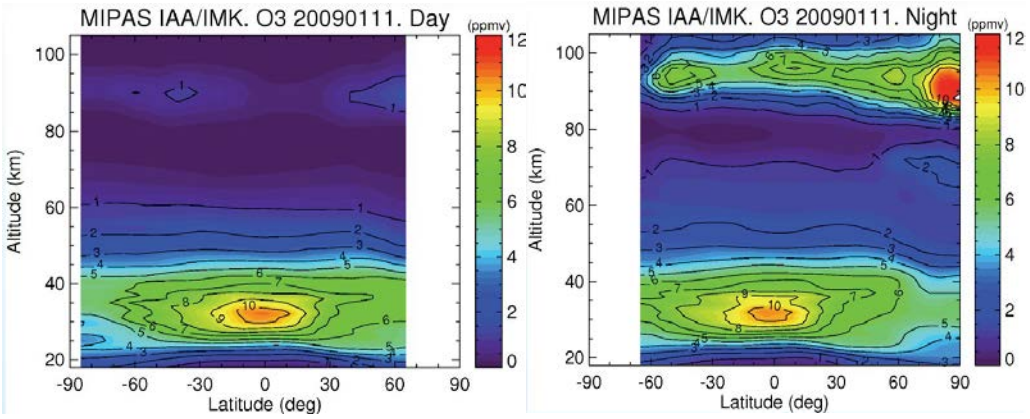

***Figure 1**: Measurements of ozone by MIPAS, left: day-time observations, right: night-time observations, 11 January 2009; unit are in ppmv. [Lopez-Puertas et al., pers. comm., 2012.]*

Vertical resolution of MIPAS ozone profiles at nighttime is 4-6 km below 95 km altitude and 6-15 km above. In daytime, the resolution is reduced to 6-15 km above 75 km. The precision of retrieved ozone profiles ranges from <20% below 90 km altitude to <40% above (Ceccherini et al., 2008).

Ozone profiles from MIPAS and **GOMOS** were compared by Verronen et al. (2005) and found to be in good agreement throughout the middle atmosphere. Nighttime ozone number density is retrieved from GOMOS observations between 20 km and 100 km altitude. The vertical resolution is 2 km below 30 km, and 3 km above. Estimated precision of mesospheric ozone profiles is 2-10% (Tamminen et al., 2010). GOMOS measurements started in April 2002 and were interrupted for short periods (May-June 2003, January-August 2005) due to problems with the instrument (Kyrölä et al., 2006; 2010).

The **ACE-FTS** ozone profiles extend from 5 to 95 km (Dupuy et al., 2009, Smith et al., 2013) with vertical resolution of 3-4 km.

SAGE II ozone measurements are available for the time frame 1984-2005. The satellite covers 60°S-60°N with a repeat cycle of slightly more than one month. Retrieved ozone profiles range up to about 70 km with 5% to 7% accuracy at 53 km (Wang et al., 2002).

A combined SAGE II-GOMOS ozone profile data set spanning the time frame 1984-2012 is also available. Coverage is 60°S-60°N, with profiles extending from 20 km to 60 km. The data is gridded 1 km in the vertical, 1 month in time, and 10° in latitude (Kyrölä et al., 2013).

Ozone profiles are retrieved from the **SCIAMACHY** instrument between 12 km and 65 km. The accuracy of retrieved ozone profiles is typically better than 10% between 20 km and 55 km and 20-30% above 55 km (Rohen et al., 2008; Mieruch et al., 2012). Data products are available for the time frame 2002-2012.

The **SMR** instrument provides ozone profiles with vertical resolution of ~3 km. The altitude range is ~9-70 km with different amounts of a priori information (Urban et al., 2005; Jégou et al., 2008).

Smith et al. (2013) published a summary of a large number of recent ozone data sets (last 10-15 years). Instruments included are: HALOE, HRDI (High Resolution Doppler Imager), SABER, GOMOS, MIPAS, OSIRIS, ACE-FTS, SOFIE, and SMILES (Superconducting Submillimeter-Wave Limb-Emission Sounder).

2.3 Observation of water vapour

A preliminary version of mesospheric water vapour retrieved from the **MIPAS** instrument is available. MIPAS measurements were acquired in the nominal mode up to 70 km and in the period of 2005-2012 up to 90 km. The vertical resolution is 4 km below 70 km, and 4-6 km between 70 km and 90 km. The typical precision of single profiles is 10% below 60 km, 20% at 60-80 km, and 50% at 80-90 km (Milz et al., 2005).

Water vapour profiles retrieved from the **ACE-FTS** instruments are available between 5 km and 101 km altitude with nearly global coverage. Validation comparisons for data product version 2.2 suggest that the uncertainties up to 70 km are less than 5% (Carleer et al., 2008). Data sets are available for the timeframe 2004-present.

The **Aura MLS** water vapour product (v.3.) is available for the period 2004-present. The scientific useful range of heights is 416 hPa to 0.002 hPa. The accuracy of retrieved water vapour profiles is estimated to be 0.2 to 0.5 ppmv (4-11%) (Nedoluha et al., 2013).

Water vapour measured by **SOFIE** is available between 50 km and 110 km altitude (as given on the project webpage).

SMR measurements cover the latitude range from 82.5°S to 82.5°N. The retrieved vertical profiles cover altogether an altitude range from about 20 km to 110 km with a typical altitude resolution of about 3 km (Urban et al., 2007; 2014). The statistical error of individual profiles can be in the order of 40% to 50% at 90 km and even exceed 100% above 100 km (Lossow et al., 2009). Hence, averaging over many profiles is necessary in order to get sensible results in the upper mesosphere.

Water vapour measurements by **HALOE** are available up to 0.01 mbar. The total error of mixing ratios is less than 27% below 0.04 mbar (Harries et al., 1996).

2.4 Observations of methane

Methane is retrieved by the **MIPAS** instrument, which has a resolution of 5 km between 70 km and 120 km (von Clarmann et al., 2009).

Measurements of methane by the **ACE-FTS** instrument are obtained between 5 and 75 km and have an estimated accuracy of within 25% from the middle stratosphere to the lower mesosphere (De Mazière et al., 2008; Waymark et al., 2013). The ACE-FTS profiles obtained

between February 2004 and August 2008 are compared to CMAM simulations by Jin et al. (2009).

The **SOFIE** data product includes profiles of methane volume mixing ratios between 40 km and 95 km altitude.

2.5 Observations of carbon oxides

CO is available from **MIPAS** over the full mission life time from the nominal mode (6 to 70 km) and for the special observation modes (up to 110 km) since 2005. The precision of individual CO profiles is typically 5–30 ppbv (15–40% for altitudes greater than 40 km and lower than 15 km and 30–90% within 15–40 km). Estimated systematic errors are in the order of 8–15%. Below 60 km, the vertical resolution is 4–7 km (Funke et al., 2009).CO_2 measurements are available from **SABER** (Mertens et al., 2001; 2004; 2009).

CO is retrieved from **ACE-FTS** spectra over the range from 5 to 110 km with a vertical resolution of 3-4 km (Clerbaux et al., 2008; Waymark et al., 2013). CO_2 is also retrieved from 60 to 120 km and, in the time range from February 2004 to August 2007, profiles of CO_2 were obtained with typical errors in the range of 2-9% in the mesosphere (Beagley et al., 2010).

CO data from **Aura MLS** are retrieved with a vertical resolution of ~2.5 km in the stratosphere and mesosphere (Waters et al., 2006; Pumphrey et al., 2007; Livesey et al., 2008).

Volume mixing ratios of CO_2 are available from the **SOFIE** experiment in the altitude range 50-100 km.

SMR observes CO in the altitude range 18-100 km with a resolution of ~3 km (Murtagh et al., 2002; Dupuy et al., 2004).

2.6 Observations of nitrogen oxides

Significant information about the NO_2 abundance is found in **MIPAS** data between 15 km and 65 km. The vertical resolution of retrieved NO_2 profiles varies between 3.5 km and 6.5 km in the 16-50 km altitude range, and increases to 9-12 km above. There is no significant difference in resolution between daytime and nighttime observations. Retrieval errors are generally below 1 ppbv above 40 km (Funke et al., 2005). In case of NO, significant information is found between 22 km and 60 km. The vertical resolution is 4-7 km between 20 and 50 km altitude, and the estimated precision of retrieved NO is generally better than 1 ppbv. At high latitudes retrieval errors were found to be up to 5 ppbv around 50 km altitude (Funke et al., 2005). Later, the retrieval of NO in the mesosphere was substantially improved and profiles are now available up to about 100 km from middle atmosphere observations, 150 km from upper atmosphere observations (Bermejo-Pantaleón et al., 2011). The single profile vertical resolution in the 70-100 km region is 15-20 km and the precision ranges from 50% at 70 km to 30% at 100 km. Systematic errors in the polar winter region amount to about 10% (Bender et al., 2014).

The **SCIAMACHY** instrument was run in a special mesosphere-lower thermosphere mode one day every two weeks from July 2008 until the end of ENVISAT in April 2012. NO density profiles were retrieved at altitudes 70-150 km with a vertical resolution of 5-10 km.

The average horizontal distance between individual observations is about 7°. Data are available on a fixed 2.5° latitude grid with vertical steps of 2 km (Bender et al., 2014).

NO and NO_2 profiles are retrieved from observations with the **ACE-FTS** instrument between ~9 and 105 km and 7 and 52 km, respectively (Kerzenmacher et al., 2008; Waymark et al., 2013).

SOFIE measures NO between 80 to 120 km altitude in the latitude band between 65 and 85 degree. SOFIE provides a vertical resolution of 1.5 km (Russell et al., 2009). Comparison with ACE-FTS show very good agreement of NO profiles for the southern hemisphere, while there is a low bias of -18.5% in the northern hemisphere (Gómez-Ramírez et al., 2013). SOFIE data is available since April 2007.

The **OSIRIS** data product of mesospheric NO consists of density profiles in the altitude range 85-100 km. In 2003-2006 OSIRIS observed the mesosphere-lower thermosphere (MLT) one day out of ten, while starting in 2007 the MLT region was sampled every other day. Climatologies of NO have been produced (Sheese et al., 2011).

From the **SMR** instrument, a 12 year-data set is available (2003 to present). NO is retrieved from a thermal emission line near 551.7 GHz in the ~30-115 km altitude range. The measurements were performed on the basis of one measurement day per month before 2007, and four days per month after this date. The vertical resolution is about 7 km. SMR is the only active instrument providing NO observations with full global coverage in the whole MLT altitude range. Bender et al. (2014) compare NO measurements in the MLT from MIPAS, SCIAMACHY, SMR and ACE-FTS. They present a multi-linear regression model obtained from the observations of these four instruments, and show that SMR NO measurements agree very well with the composite fit, with a slight high bias of 8% on average.

GOMOS NO_2 profiles are typically available up to 50-55 km in normal conditions (Kyrölä et al., 2010), and extend up to 65-70 km in perturbed conditions (solar storms, see Seppälä et al., 2007). The vertical resolution after Tikhonov-type regularization is 4 km (Tamminen et al. 2010). Data are available between 2002 and 2012.

HALOE measured NO from the lower stratosphere up to 130 km and NO_2 in the stratosphere (Gordley et al., 1996). Hood and Soukharev (2006) analyzed NO data from HALOE for the time frame 1991-2003.

Datasets of NO in the lower thermosphere are retrieved from observations carried out with the Student Nitric Oxide Explorer (**SNOE**) satellite and the **Solar Mesospheric Explorer** (Barth et al., 2003; Barth et al., 1988).

2.7 Observations of Polar Mesospheric Clouds (PMCs)

Starting from the 1970s, polar mesospheric clouds (PMCs) have been observed with several satellite sensors which were originally designed to observe other atmospheric species. This era started with measurements on the Orbiting Geophysical Observatory (**OGO-6**) which applied limb scattering at visible wavelengths (Donahue et al., 1972). Starting from these seminal observations, PMCs and their global features have been studied from more than 16 different satellite platforms (see DeLand et al., 2006 for a review of these observations). The longest PMC observations were made by the **SBUV** instruments (DeLand, 2003).

The AIM satellite is specifically designed to study PMC. The **SOFIE** instrument is used to derive PMC particle properties (Hervig et al., 2009). The **CIPS** camera makes high-resolution

spatial images of PMC (Chandran et al., 2009). With the instrumentation on AIM, PMC abundances, spatial distribution, particle size distributions, gravity wave activity, dust influx into the atmosphere and vertical profiles of temperature, H_2O, OH, CH_4, O_3, CO_2, NO, and aerosols are measured.

Pérot (2010) published PMC altitude and brightness retrieved from observations with the limb-viewing **GOMOS** stellar occultation experiment. The time frame covered in this study is 2002-2006.

PMC brightness, altitude and particle sizes are derived from **OSIRIS** (von Savigny et al., 2005, Petelina et al., 2005, 2006a, 2006b, 2007). The OSIRIS dataset is available since 2001.

The particle shape and radii were investigated using **ACE-FTS** spectra (Eremenko et al., 2005). The temperature of PMC particles was derived using a direct method by Petelina and Zasetsky (2009, 2011).

López-Puertas et al. (2009) report on PMC observations by the **MIPAS** instrument.

The **SCIAMACHY** instrument detects PMC and was used to derive particle size (von Savigny, 2004).

A long dataset (the time series started in 1991) is available from the **HALOE** instrument (Wrotny, 2006).

3 Available modelled mesospheric data

Changes in the mesosphere should contain clear signals of climate change, and there is increasing evidence that accurate simulations of changes to the Earth's climate require models with a well-resolved and accurate stratosphere and mesosphere (e.g., see Akmaev, 2011; Hurrell et al., 2013). Coupling exists between all regions of the atmosphere in terms of mass, momentum, and energy exchange; an understanding of the processes which occur in the middle atmosphere will provide a better understanding of the Earth atmosphere as a whole.

In the following we present an overview of general circulation models (GCMs) which are/have been used to study the mesosphere. These models are often coupled with modules for calculations of atmospheric chemistry. Inter-comparisons between different climate models are provided by Austin et al. (2008), Austin et al. (2003) and Eyring et al. (2006).

WACCM

The Whole Atmosphere Community Climate Model (WACCM) is a global chemistry-climate model (Garcia et al., 2007; Marsh et al., 2013). It incorporates the physical Community Atmospheric Model (CAM) (Neale et al., 2013). Model versions currently used are version 3 or version 4. In addition to CAM, WACCM includes parameterizations of radiative heating, molecular diffusion, and ion drag. Separate parameterizations for orographic and non-orographic gravity waves are implemented. WACCM has 66 vertical levels from the ground to 140 km and a horizontal resolution of 1.9° in latitude and 2.5° in longitude. The vertical resolution is variable and ranges between 1.1 km and 3.5 km. The spectral range covered by eight radiation bands is 170-700 nm. The time step for physical parameterizations is 1800 s. Garcia et al. (2007) studied middle atmosphere trends in a 54-year simulation from 1950 to 2003. A climate study covering years 1850-2005 is presented by Marsh et al. (2013). Smith et al. (2011) studied the mean circulation and trace species transport in the winter mesosphere.

HAMMONIA

The Hamburg Model of the Neutral and Ionized Atmosphere (HAMMONIA) is a T31 spectral model extending from the ground to ~250 km using 67 vertical levels. The vertical resolution is 2-3 km. HAMMONIA is an extension of the MAECHAM5 model. In terms of dynamics and radiation, HAMMONIA is coupled to a chemical module including 48 compounds and 148 gas phase reactions. Dynamical and radiative processes implemented in HAMMONIA include solar heating at UV and EUV wavelengths, non-local thermodynamic equilibrium long-wave radiation, heating and mixing due to gravity waves, vertical molecular diffusion and heat conduction, as well as a parameterization of electromagnetic forces in the thermosphere (Schmidt et al., 2006). 20-year runs of HAMMONIA were used by Beig et al. (2012) to assess the 11-year solar cycle response in mesospheric ozone and temperature.

CMAM

The extended Canadian Middle Atmosphere Model (CMAM) is a T42 spectral general circulation model with 70 levels end extends from ground to about 210 km. The original CMAM model is characterized by Beagley et al. (1997). The extension for the mesosphere includes non-LTE parameterizations for the 15-μm CO_2 band, solar heating due to absorption

by O_2 in the Schumann-Runge bands and continuum, and by O_2, N_2 and O in the EUV spectral region, parameterized chemical heating, molecular diffusion and viscosity, ion drag and a modified non-orographic gravity-wave drag (GWD) scheme (Fomichev et al., 2002; McLandress et al., 2006). The model describes the neutral atmosphere. The region above 120 km is considered a deep viscous layer for dissipating upward propagating waves. The horizontal resolution is 6°, and in the mesosphere, the vertical resolution is 3 km. The model covers the spectral range 250-680 nm. A chemistry model containing 44 species and 127 photochemical reactions can be included. A 33-year simulation of CMAM was used for ozone climatology studies (de Grandpré et al., 2000). Present CMAM simulations cover the period 1960-2004.

FUB-CMAM

The Freie Universität Berlin Climate Middle Atmosphere Model (FUB-CMAM) is a T21 spectral general circulation model extending from ground to ~83 km. The horizontal resolution is 5.6°x5.6°, and the vertical resolution is 3.5 km in the middle atmosphere. The physical processes represented in the model include the hydrological cycle, a radiation scheme, vertical diffusion and a weak linear Rayleigh friction in the upper mesosphere instead of a gravity wave parameterization. Absorption and emission of shortwave and longwave radiation due to ozone, water vapor and CO_2 is modelled (Matthes et al., 2004).

EMAC

The ECHAM/MESSy Atmospheric Chemistry (EMAC) model is a numerical chemistry and climate simulation system that includes sub-models describing tropospheric and middle atmosphere processes and their interaction with oceans, land and human influences (Jöckel et al., 2006). It uses the Modular Earth Submodel System (MESSy) to link multi-institutional computer codes. The core atmospheric model is the 5th generation European Centre Hamburg general circulation model (ECHAM5, Roeckner et al., 2006). EMAC is available in different horizontal and vertical resolution, e.g. the T42L90MA-configuration, i.e. with a spherical truncation of T42 (corresponding to a quadratic Gaussian grid of approx. 2.8°x2.8° in latitude and longitude) with 90 vertical hybrid pressure levels up to 0.01 hPa (approx. 80 km altitude).

The REF-C1SD (Reference C1, Specified Dynamics) simulation is the starting point for model evaluation studies and scientific investigations. It is part of the ESCiMo (Earth System Chemistry integrated Modelling) project, a contribution to the SPARC/IGAC CCMI (Chemistry Climate Modelling Initiative). REF-C1SD is executed with T42L90 resolution (with a 12 minutes time step). This simulation uses specified dynamics ("SD"), i.e. nudging the dynamic fields coming from re-analyses, but only up to 10 hPa (i.e. about 30 km). The relaxation was performed every six hours with a maximum nudging height at layer 37 (10 hPa, i.e. about 30 km), where top of the atmosphere is layer 1 (at 0.01 hPa, i.e. 80 km), using ERA-Interim data (see Berrisford et al., 2009, 2011; Dee et al., 2011). Nudged entities are divergence, vorticity, temperature (low modes, without global mean) and the logarithm of the surface pressure. Additional boundary conditions that were provided by ERA-Interim are: Sea Surface Temperatures (SSTs) and Sea Ice Cover (SIC). For the altitudes above 30 km, the model is running "free", meaning that the upper stratosphere and mesosphere is creating their own dynamical structure in a consistent manner. For all heights, from the surface up to the upper boundary (near 80 km), the chemical fields are calculated in a consistent manner. Besides the consideration of the 11-year solar cycle (based on observations of the 10.7 cm flux), there are no specific forcings in the mesosphere. The REF-C1SD simulation provides a

good foundation for analyses regarding climatological features and short- and long-term fluctuations of temperature and chemical composition in the mesosphere.

So far, the REF-C1SD simulation covers the period 1979-2012. The REF-C1SD simulation is started in 1979 as a branch from the free running REF-C1 simulation, which covers the period 1950-2012. REF-C1 and REF-C1SD offline emissions have a 0.5°x 0.5°resolution with monthly data for the years 1950-2012. They include emissions from the sectors: Land (w/o agricultural waste burning (AWB), road), road, AWB, Ship, Air. From 1960 to 2000 the MACCity (data description and access via //eccad.sedoo.fr/, additional information Granier et al., 2011) data set, which is based on the ACCMIP emission inventory (Lamarque et al., 2010) are used. As the ACCMIP emission inventory stops at the end of 2000, the IPCC RCP 8.5 scenario is used instead, in particular for the years from 2005 to 2010, as it is the nearest scenario which can be added to ACCMIP-data and which should be consistent with expected changes. Between 1960 and 2010 the emission were linearly interpolated and a daily emission cycle was applied. The 1950-1959 emissions are assumed to be constant and set to the value of 1960. The years 2011 and 2012 are included using the same emissions as for 2010.

TIME-GCM

The thermosphere-ionosphere-mesosphere-electrodynamics general circulation model (TIME-GCM) is a GCM covering the altitude range 30-500 km (Roble and Ridley, 1994). The model includes physical and chemical processes appropriate for the mesosphere and upper stratosphere. TIME-GCM is used to study the global circulation, temperature and compositional structure for equinox, solar cycle minimum, geomagnetic quiet conditions.

EUGCM

The extended UGAMP general circulation model (Norton and Thuburn, 1997) has an upper boundary near 125 km. UGAMP stands for the UK Universities' Global Atmospheric Modelling Program. It was used to study relations between gravity wave drag and planetary waves in the mesosphere.

SKYHI

The Geophysical Fluid Dynamics Laboratory SKYHI is a finite-difference general circulation model that extends from the ground to 80 km altitude (Hamilton, 1995). It contains 40 vertical levels with 3 km vertical resolution in the mesosphere. The minimal horizontal resolution is 1° x 1.2° (or 3° x 3.6° for longer simulations). SKYHI models radiative transfer and the hydrological cycle (Koshyk and Hamilton, 2001) and is used also for stratospheric studies (Hamilton, 2001). The study by Erlick et al. (2006) was based on a 25-year run.

GISS

The Goddard Institute for Space Studies (GISS) models are a series of coupled chemistry-climate general circulation models. The maximum resolution is 2° x 2.5° in latitude/longitude and 2-3 km vertical in the mesosphere (Rind et al., 1988; Rind et al., 2007). The highest altitude is 85 km. The models include calculation of radiative and surface fluxes and the hydrological cycle. A gravity wave parameterization was added to the basic model. GISS simulations for the time frame 1959–2067 were analyzed by Shindell (1998). Climate runs between 1880 and 2003 were studied by Hansen et al. (1999) and Hansen et al. (2007).

MRI

MRI is a coupled chemistry-climate model (CCM). The spectral general circulation model (GCM) with 45 levels reaches up to an altitude of ~80 km (Shibata and Deushi, 2005). The horizontal resolution is 2.8° and the vertical resolution in the stratosphere is 2 km. Modelled processes include convection, radiation, the planetary boundary layer and the hydrological cycle. The chemical module includes 49 stratospheric species, and 43 chemical reactions, among them reactions on polar stratospheric clouds and sulfate aerosols.

UMETRAC

UMETRAC is a coupled chemistry-climate model based on Met Office's Unified Model (UM). The model extends from the ground to 80 km at a resolution of 2.5° x 3.75° in latitude/longitude. UMETRAC includes tracers relevant for stratospheric chemistry and photochemical processes as well as a gravity wave parameterization. Simulations include the time range 1975-2020 (Austin, 2003). Struthers et al. (2004) used UMETRAC to quantify the rates of increase in NO_2.

CCSR/NIES

The Center for Climate System Research/National Institute for Environmental Studies (CCSR/NIES) CGCM is a T21 spectral model with 34 levels that extends up 70-80 km altitude. The horizontal resolution is 5.6°. CCSR/NIES includes an oceanic part and the flux of ocean-atmosphere heat and water exchange is considered. It is used for greenhouse gas studies (Akiyoshi et al., 2004). Climate simulations include the time range 1986-2050.

4 Status of present understanding

The mesosphere covers the altitude range from 50 to 100 km; it is a complex, yet least explored layer of the atmosphere regarding climate change effects. It is around two decades since climate scientists began to calculate how the greenhouse effect might influence also the mesosphere (e.g., Berger and Dameris, 1993). This region gradually became an important region to the climate change debate because the magnitude of change predicted for this region is expected to be larger than at lower altitudes and poses a significant relevance to weather and climate. However, relatively little was known about how the upper part of the middle atmosphere will respond to these climate forcing parameters. Several measurements and model calculations have made it increasingly clear that releases of trace gases from human activity have a potential for causing a change in the present-day climate of Earth (e.g., Beig, 2011).

So far rocket soundings and satellite monitoring have highlighted the strong variations that occur as a function of height in the physics and in the chemical composition. For example, as the altitude increases through the mesosphere, strong vertical mixing conditions that maintain the mixing ratio of long-lived species relatively constant with height are progressively replaced by conditions in which molecular diffusion prevails, leading to gravitational separation of chemical species according to their respective mass. The fast change with height in the amount of solar radiation available photolysing atmospheric molecules also leads to a prompt chemical transition in the mesosphere. The major contributions to the energy budget in the mesosphere are provided by solar heating resulting from ozone absorption, emission of infrared radiation by CO_2, adiabatic processes, and the transport of heat through advection.

The deposition of momentum from upward propagating waves provides the major forcing mechanism for the meridional circulation of the middle atmosphere. The dissipation of small-scale gravity waves produces a body force on the zonal flow, leading even to a reversal of the zonal wind in the vicinity of the mesopause. Simultaneously, this momentum source produces a mesospheric circulation directed from the summer pole to the winter pole, and through mass continuity gives rise to ascending and descending motions in the summer and winter hemispheres, respectively. Other wave motions also have strong effects on the structure of the middle atmosphere, including diurnal and semi-diurnal tides, which produce periodic fluctuations in temperature, wind components and species concentrations, planetary waves (e.g., Rossby waves), and equatorial waves (Kelvin waves and mixed-Rossby gravity waves) which are (together with small-scale gravity waves) believed to drive the observed semi-annual and quasi-biennial oscillations (SAO and QBO). The sources of these waves are mainly located in the troposphere or near the Earth surface; their ability to reach the middle atmosphere depends on filtering and dissipation mechanisms of the atmosphere itself (Charney and Drazin, 1961).

Natural variations and human-induced changes to be expected in the mesosphere cannot be assessed without understanding the dynamical, radiative and chemical couplings existing between the different layers of the atmosphere. In recent years, many chemistry-climate models (CCMs) have been developed extending from the surface to the mesosphere (mostly with an upper boundary at 0.01 hPa / 80 km); some efforts are undertaken to consider the complete mesosphere and the lower thermosphere (up to 120 or 150 km).

4.1 Observed mesospheric data

Temperature observations

Beig et al. (2003) and Beig (2006; 2011) have summarised the knowledge at that time on mesospheric temperature trends. The measurements reported during the past few decades suggested that strong changes in upper atmosphere structure are occurring much faster than model predictions and have latitudinal as well as longitudinal variations, indicating that there is an important need to understand their long-term variability. They showed that the mesosphere cooling between 50 and 80 km amounts to about 2 K/decade obtained from datasets from the 1960s to date (see below Table 4 in Beig et al., 2003). However, at that time no obvious cooling trend is found in the mesopause region (i.e. 80 to 100 km; see below Table 5 in Beig et al., 2003). Analyses using results of long-term low-frequency measurements have shown that mesospheric cooling is not linear. In particular, a correlation is found between MLT temperatures and stratospheric ozone (Bremer et al., 2008), which plays a major role in the middle atmosphere energetics. Changes in temperature affect the wind field and vice versa. The winds in the mesosphere are usually estimated from temperature data collected by satellites but also direct wind observations have been made, most notably by WINDII (Shepherd et al., 1993; McLandress et al., 1996). The winds at these high levels are assumed to be geostrophic. Recent results on long-term changes in mesospheric (and lower thermosphere) winds have been published by Jacobi et al. (2006) and Portnyagin et al. (2006). They showed that observed wind parameters have significantly changed since the beginning of the early 1960s.

Table 4. Temperature Trend in the Mesosphere (50–79 km) Region

Reference	*Technique*[a]	*Years of Analysis*	*Location*	*Height, km*	*Temperature Trend, K/decade*
Angell [1991]	U.S. rocketsonde	1973–1985	8°S–55°N	50–55	−2.5
Dunkerton et al. [1998]	U.S. rocketsonde	1962–1991	8.6°S–37.5°N	50–60	−2.5 to −4.5
Keckhut et al. [1999]	U.S. rocketsonde	1969–1995	(8°S to 34°N) and (14°W to 167°W)	60 65–75	−3.3 (±0.9) −2.2 (±2)
Beig and Fadnavis [2001]	Indian rocketsonde	1971–1993	8.5°N, 77°E	50 60 70	−1.5 (±0.8) −3 (±1.3) −5.6 (±1.7)
Golitsyn et al. [1996]	Russian rocketsonde	1965/1969–1995	midlatitudes: (49°N, 44°E) and (47°N, 75°E)	50–60 70	−3.5 to −8.8 (±1.15) −5.2 (±1.30)
Golitsyn et al. [1996]	Russian rocketsonde	1964/1969–1995	high latitudes: (81°N, 58°E) and (68°S, 46°E)	50–60 70	−2 to −3.5 (±1.10) −10 (±2.05)
Komuro [1989] and *Keckhut and Kodera* [1999]	Japanese rocketsonde	1970–1989 1970–1995	39°N, 141.5°E	20–55	−2.5 (±1.1)
Lübken [2000, 2001]	rocket grenade and falling sphere	1987–2000	69°N, 10°E	50–85	−0.24 (±0.14) (summer)
Aikin et al. [1991]	satellite SSU channel and French lidar data	1980–1990	44°N, 6°E	55	−1.5 to −2
Keckhut et al. [1999]	Rayleigh Lidar	1979–2001	44°N, 6°E	65 75	−3 (± 2.2) −2 (± 2.5)
Remsberg et al. [2002]	UARS, HALOE-SR, and SS (satellite)	1991–2001	tropics and 20°N	50–62	−1.0 to −1.6

[a]SSU is stratospheric sounding unit; SR is sunrise; and SS is sunset.

Table 5. Temperature Trends in the Mesopause Region (80–100 km)

Reference	Technique	Years of Analysis	Location	Height, km	Temperature Trend, K/decade	Remarks
			Direct Measurements: Hydroxyl Airglow Rotational Temperature Technique			
Semenov and Shefov [1999]	hydroxyl rotational temperature bands: several	1957–2000	(42°–56°N) and (37°–43°E)	mean OH emission layer height (87 ± 8 km)	−6.8 (±1)	
Burns et al. [2002] and *French* [2002]	hydroxyl rotational temperature, band: 6-2	1990, 1995–2001	69°S, 78°E	mean OH emission layer height (87 ± 8 km)	no discernible trend	
Offermann et al. [2003]	hydroxyl rotational temperature band: 3-1	1980–1998	51.3°N, 7°E	mean OH emission layer height (87 ± 8 km)	+0.2 (±0.9)	
Lowe [1999, 2002]	hydroxyl rotational temperature band: 3-1	1989–2001	43°N, 81°W	mean OH emission layer height (87 ± 8 km)	+0.6 (±2.3)	
Espy and Stegman [2002]	hydroxyl rotational temperature band: 3-1	1991–2001	59.5°N, 18°E	mean OH emission layer height (87 ± 8 km)	5 (±2.0) (winter) no trend (summer)	
Reisin and Scheer [2002]	hydroxyl rotational temperature band: 6-2	1986, 1987, 1992, 1997–2001	31.8°S, 69.2°W	mean OH emission layer height (87 ± 8 km)	−10.5 (±0.8)	
Sigernes et al. [2003]	hydroxyl rotational temperature band: 6-2 band: 8-3	1983–2001 1980–1983	78°N, 15°E	mean OH emission layer height (87 ± 8 km)	+0.3 (±1.0) (winter)	
Semenov et al. [2002]	combined (major: hydroxyl rotational temperature bands: several)	1957–1976, 1984–1986, 1990–2000	41.8°N, 43°E and 55.7°N, 37°E	mean OH emission layer height (87 ± 8 km)	+0.3 (±0.8) (summer) −9 (±1.2) (winter)	
H. Takahashi (unpublished data, 2002)	hydroxyl rotational temperature band: 6-2	1994–2002	23°S, 45°W	mean OH emission layer height (87 ± 8 km)	not available	analysis under process
			Direct Measurements: Other Techniques			
Remsberg et al. [2002]	UARS –HALOE -SR and SS (satellite)	1991–2001	45° to 45°N	80	no significant trend	
Lübken [2000, 2001]	rocket grenade and falling sphere	1987–2000	69°N, 10°E	50–85	−0.24 (±0.14) (summer)	
Reisin and Scheer [2002]	O_2 rotational temperature	1986–2000	31.8°S, 69.2°W	95	−0.3 (±1.5)	
She and Krueger [2003]	Na lidar	1990–1999	41°N, 105°W	92	0.0 (±2.5)	error limits represent 1σ error
Semenov [1997] and *Semenov et al.* [2002]	atomic oxygen line in 557.7 nm data	1965–1974	40°N, 106°W	97	−1 (±1)	
			Indirect Measurements			
Clemesha et al. [1992, 1997]	centroid height of sodium emission	1972–1987	23°S, 45°W	20–92	−1.5	
Fishkova et al. [2001]; *Semenov et al.* [2002]	intensity of the sodium emission	1957–1992	41.8°N, 43°E	92	no trend (winter)	
Bremer [1997] and *Bremer and Berger* [2002]	ionospheric reflection height	1964–1995	51°N, 7°E	48–82	−1.4 to −2.1	
Taubenheim et al. [1997]	low-frequency radio signal reflection height data	1961–1997	51°N, 7°E	50–80	−6 (summer)	
Nestorov et al. [1991]	A-3 radio wave absorption	1959–1986	45°N, 13°E	mesosphere	−1.93	
Gadsden [1990] and *Gadsden* [1997, 1998]	occurrence frequency of noctilucent clouds	1964–1982 and 1964–1995	(54°–58°N) and (20°E–11°W)	82	−2.5	

Table 2. Taken from Beig et al., 2003.

In the tropics, results have been discussed derived from a few reliable data sets from lidar and satellite for the past two decades (Beig, 2011). These new tropical trend analyses indicate a cooling trend over the last 20 years, but magnitude is found to be smaller than the earlier results reported mainly from rocketsonde measurements carried out during the late 1960s to early 1990s (see above tables). This cooling trend increases with height in the mesosphere and becomes around 3 K/decade around 70 km but with an uncertainty of about 1-2 K/decade. The mesospheric temperature trends for the midlatitudes are consistent with the earlier conclusion of a cooling of a few degrees per decade in the lower mesosphere and middle mesosphere. The most noticeable addition in the mesospheric temperature trend research is the robust analysis of HALOE data (here 1991-2005). The cooling trends from the HALOE data set are found to be significant at most latitudes of the middle and lower mesosphere. They range from −1 K/decade at low latitudes to about −3 K/decade at the middle latitudes (Remsberg, 2008; 2009). Values of the order of −1 K/decade are reasonably consistent with those reported from the lidar measurements at low latitudes. At middle latitudes, there is reasonable agreement in the middle and upper mesosphere with published values from rocket sondes and lidar measurements of the preceding two decades. However, the HALOE trends are smaller in the lower mesosphere. This later may be due to the fact that earlier comparative results were obtained when the decreasing upper stratosphere ozone was an added factor for the total radiative cooling response at those altitudes. The cooling trend diagnosed from HALOE, are generally larger than those from models for the middle latitudes of the upper mesosphere.

The role of dynamics, particularly the role of small-scale gravity waves and its breaking (deposition of energy and momentum), is very important to better understand the temperature trend features. The present knowledge on the parameterisation of gravity wave effects in the middle atmosphere is far from satisfactory (Fritts and Alexander, 2003). Gravity wave breaking affects effectively the distributions of chemical species and the vertical diffusive transport of heat in the upper mesosphere (and lower thermosphere) region. Dissipation of gravity waves leads to heating due to the energy deposition. Strengthening of the gravity wave drag and related momentum deposition is the driver of the global mesospheric residual circulation, causing a significant cooling of the summer polar mesopause. The combined effects of enhanced greenhouse gas concentrations and of the gravity wave drag and diffusion strengthening may be a major cause of the observed distinct long-term trend in temperature of the mesospheric region. Indeed, trends of gravity wave activity in the upper mesosphere over the past 20 years have been observed at a few selected ground based stations (e.g., Hoffmann et al., 2011). However, information on corresponding global features are so far missing as well as a clear cause effect reasoning even though some initial model studies suggest a strengthening Lorentz energy cycle in a changing climate as the underlying mechanism for increasing gravity wave activity (Becker, 2009).

In the winter polar mesosphere, strong cooling events may occur at irregular intervals. These events accompany sudden stratospheric warmings (SSWs) and last usually several days. The link between SSWs and mesospheric coolings was first shown in a model study by Matsuno (1971). Several other studies investigated the mesospheric response to SSWs in circulation models (e.g. Liu and Roble, 2002; Siskind et al., 2010) and observations (e.g. Whiteway and Carswell, 1994; Walterscheid et al., 2000). Major sudden stratospheric warmings are generally confined to the northern hemisphere due to the orography which facilitates generation of planetary waves. So far there has been observed only one major warming in the southern hemisphere (Dowdy et al. 2004).

Observation of ozone

Since many years the basics of mesospheric ozone chemistry are understood; it is well known that the chemistry of ozone in the mesosphere is related to the chemistry of other oxygen/hydrogen-containing species, which must be considered concurrently (Allen et al., 1984; Vaughan, 1984). The ozone secondary maximum results from the onset of the coupling between active-hydrogen and active-oxygen chemistry and its observed variability may be a consequence of secular changes in mesopause dynamics. Allen and colleagues pointed out the significance of oxygen and hydrogen-containing species and the temperature profile on the diurnal variability of ozone. Several other studies investigated diurnal ozone variations in the mesosphere, including nighttime, with satellites (Ricaud et al., 1996; Marsh et al., 2002; Huang et al., 2008; 2010; Smith et al., 2008; 2013; 2015) and ground-based observations (Connor et al., 1994; Haefele et al., 2008). A diurnal pattern and a semi-annual oscillation (SAO) signal are seen above 50 km altitude. All of the above mentioned studies show that with nightfall when the photo-destruction of ozone stops, ozone quickly reaches a high nighttime equilibrium in the mesosphere. The photochemical models used by Ricaud et al. (1996) and Sinnhuber et al. (2003) did not show any variations during night, and observations showed little to no variations.

The tertiary maximum in ozone mixing ratio profiles reported first by Marsh et al. (2001) is observed at ~72 km altitude near the polar night terminator. Modeling results have shown that the maximum is caused by low concentrations of odd-hydrogen and the subsequent decrease

in odd-oxygen losses through catalytic cycles involving hydroxyl. The spatio-temporal distribution of tertiary ozone maximum has been studied by Degenstein et al. (2005), Smith et al. (2009), Sofieva et al. (2009), Damiani et al. (2010) and Kyrölä et al. (2010) using satellite measurements by OSIRIS, SABER, GOMOS and MLS, and by Hartogh et al. (2004; 2011) using ground-based observations. These studies have shown that the distributions of tertiary ozone maximum have specific features, which are variable from year to year. In particular, due to a long lifetime of ozone in polar night conditions, the downward transport of polar air by the meridional circulation is clearly observed in the tertiary ozone maximum time series. Although the maximum tertiary ozone mixing ratio is achieved close to the polar night terminator (as predicted by the theory), elevated ozone mixing ratios can be observed also at very high latitudes, not only in the beginning and at the end, but also in the middle of winter.

Since ozone in the mesosphere is very sensitive to HO_x concentrations, energetic particle precipitation can significantly modify the shape of the ozone profiles (Seppälä et al., 2006; Sofieva et al., 2009).

The modelling of tertiary ozone maximum is challenging, because it is affected by chemistry, dynamics, and energetic particle precipitation (Sofieva et al., 2009; Verronen et al., 2013). Therefore, comparison of experimental and simulated tertiary ozone maximum distributions is a good test for validation/optimization of chemistry-transport models.

For the first time, trends of ozone and temperature measured at the same times and locations are obtained (from the SABER instrument, from 2002 to this day (i.e. end 2014), from 20 to 100 km altitude, 48°S to 48°N latitude); their correlations provide some useful information about the relative importance of photochemistry versus dynamics over the longer term (Huang et al., 2014, see their Fig. 2 reproduced below in Fig. 2). In the mesosphere region from 50 to 80 km, the ozone trends are mostly flat, with indications of small positive trends at lower latitudes. The temperature trends in this region are mostly negative, showing decreases of up to about −3 K/decade. Remsberg (2009) presented mesospheric ozone trends based on data from the HALOE experiment which are in agreement with Huang et al. (2014): Between 50 and 60 km at low latitudes, the trend values are essentially zero. Negative trends of about 2%/decade to 4%/decade are found at midlatitudes near 50 km. In upper mesosphere (above 90 km), the temperature and ozone trends are both negative. The ozone trend can reach approximately −10%/decade as altitude increase, and the temperature trend can reach −3 K/decade. Above 90 km, the ozone and temperature trends are positively correlated, while between 80-90 km they appear to be anti-correlated.

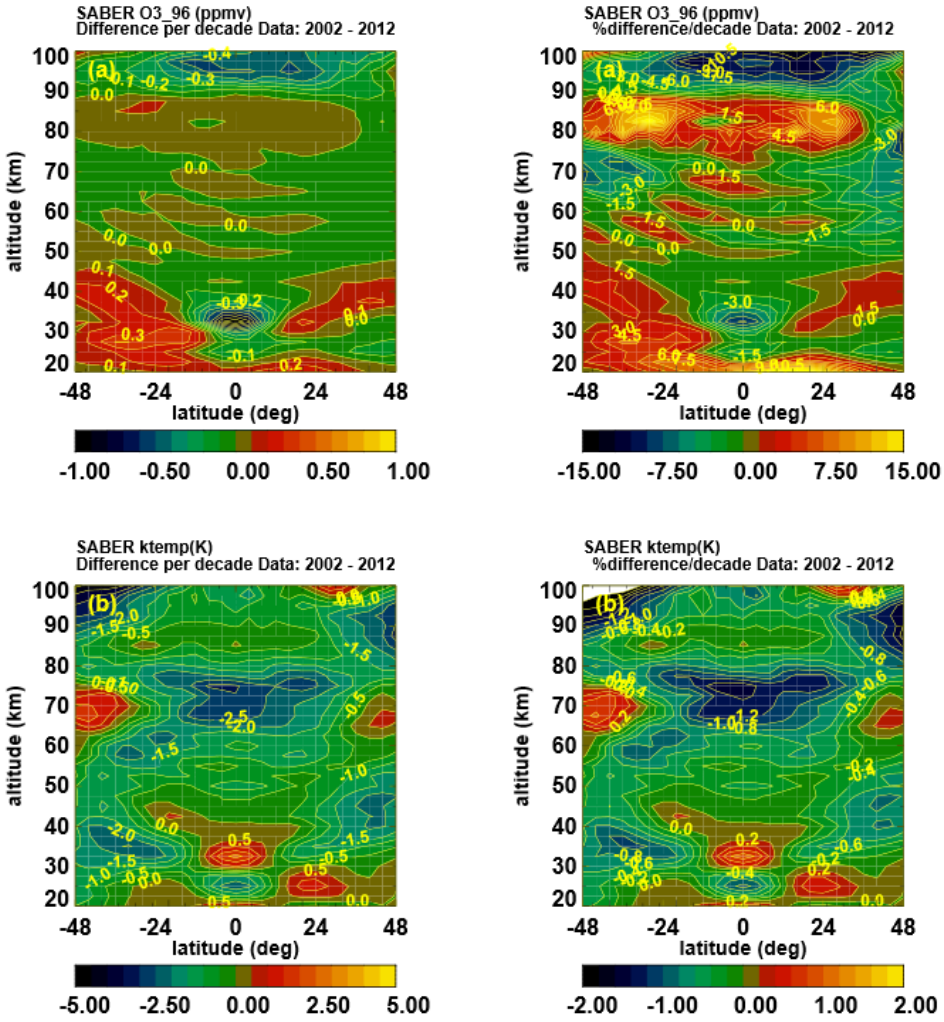

Figure 2. Ozone and temperature trends on altitude (20 to 100 km) vs. latitude (48° S to 48° N) coordinates. Top row left: ozone differences (ppmv) (2012–2002); right: percent differences. Bottom row: as in top row, but for temperature (K). Brown-green borders denote zero contours, with brown and red areas denoting positive trends.

Figure 2. Taken from Huang et al., 2014.

Observation of water vapour

In the recent 3 decades a series of satellite-borne and ground-based measurements have established a general picture of the water vapour distribution in the middle atmosphere (e.g., Taylor et al., 1981; Fischer et al., 1981; Remsberg et al., 1984; Reber et al., 1993; Mote et al., 1996; Nedoluha et al., 1996; Summers et al., 1997; Chandra et al., 1997; Randel et al., 1998; Seele and Hartogh, 1999; Summers et al., 2001; Hervig et al., 2003; Thomason et al., 2004; Nassar et al., 2005; Randel et al., 2006; Urban et al., 2007; Lossow et al., 2008; 2009; Hurst et al., 2011; Randel and Jensen, 2013).

The middle atmospheric circulation leads to reduced water vapour mixing ratios in the mesosphere of the winter pole due to descent motion from the mesopause and enhanced the water vapour amount in the summer pole mesosphere due to upward transport of H_2O rich air. This seasonal variation of the global wind system is certainly the major cause of the observed large variability of mesospheric water vapour, which is characterised by an annual variation at the poles which gradually changes towards a semi-annual cycle in the tropics.

As the most abundant source of chemically active HO_x radicals (H, OH, HO_2), water vapour has a direct impact on the photochemical cycles and the composition of the entire middle atmosphere. Water vapour is involved in the build-up of polar mesospheric clouds (PMCs), also known as noctilucent clouds (NLCs) at the summer mesopause. In the stratosphere H_2O mixing ratios increases again with height due to the formation from oxidation of methane and reaches a maximum at the stratopause and lower mesosphere. The chemical lifetime of water vapour in the middle atmosphere is of the order of years in the lower stratosphere and months in the lower mesosphere (Brasseur and Solomon, 2005), allowing for water vapour to be used as a tracer in the upper stratosphere and lower mesosphere. Through the formation of hydrogen radicals, water vapour exerts a major control on the spatial and temporal distribution of chemically active species in the mesosphere and lower thermosphere region, reflected by diurnal and seasonal cycles, as well as by longer term variations such as those governed by the 11-year cycle of solar activity. For example in case of particle precipitation reaching the mesosphere, the HO_x radicals produced from H2O have a profound impact on ozone on a range of time scales (Verronen et al., 2006, Andersson et al., 2014).

Odin/SMR measurements indicate clear seasonal differences between the two hemispheres in the subtropical region. Higher water vapour concentrations are observed during summer and lower concentrations during winter in the Northern Hemisphere as compared to the Southern Hemisphere. This observation can be made roughly in the altitude range between 60 km and 90 km (Lossow et al., 2008).

Odin's water vapour measurements in the middle atmosphere show that the Semi-Annual Oscillation (SAO) is the dominant pattern of variability in the entire altitude range between 65 km and 100 km in the tropics and subtropics (Lossow et al., 2008). Maximum volume mixing ratios occur near the equinoxes below 75 km and around the solstices above 80 km. It is shown that the SAO exhibits a distinct phase change between 75 km and 80 km in the tropical region (Lossow et al., 2008). This feature can also be observed in the temperature distribution, where the transition occurs somewhat higher in altitude (see Huang et al., 2006). In comparison to the HALOE analysis of the mesospheric SAO in water vapour (Jackson et al., 1998) the water vapour maxima observed by Odin/SMR occur one month earlier. (So far the reason is unknown.)

The tropical water vapour profile is characterised by an increase with altitude due to methane oxidation, a maximum in the upper stratosphere and lower mesosphere and a decrease above 65 km, depending on season. Due to the relatively long photochemical lifetime of water vapour, its global distribution depends strongly on the seasonal variation of the meridional circulation with large scale ascending and descending motions in the summer and winter hemisphere, respectively, and a reversal observable in autumn and spring.

Thornton et al. (2009) presented results from the first detailed intercomparison of stratosphere-lower mesosphere water vapour analyses; it builds on earlier results from the EU funded framework V “Assimilation of ENVISAT Data” (ASSET) project. With the availability of high resolution, good quality Michelson Interferometer for Passive Atmospheric Sounding (MIPAS) water vapour profiles, the ability of four different atmospheric models to assimilate these data was tested for September 2003.

Observations of nitrogen oxides

The influence of nitrogen oxides on the atmospheric ozone content was mentioned for the first time by Crutzen (1970) in his famous paper.

A major source of nitric oxides NO_x (= NO + NO_2) in the high latitude mesosphere and lower thermosphere (MLT) is through Energetic Particle Precipitation (EPP) (Barth, 1992). NO_x in the MLT is produced by dissociation of molecular nitrogen by solar photons and energetic particles, in particular auroral and precipitating electrons from the outer trapping region of the magnetosphere, and subsequent reaction of N with oxygen to form NO. Polar region nitric oxide (NO) near 110 km is well understood to be produced through EPP resulting from geomagnetic activity. In addition to thermospheric production, NO_x can be produced directly in the mesosphere and upper stratosphere during impulsive events such as solar proton events (Seppälä et al., 2004). If NO_x produced in the MLT region is transported to the stratosphere, it has significant impacts on ozone abundances there because NO is a catalytic destroyer of ozone (Bailey et al., 2014, Funke et al., 2014b and Seppälä et al., 2007).

Funke et al. (2011) have studied the atmospheric response to a strong solar proton event (SPE) using a number of trace gas species retrieved by MIPAS and compared with a large number of atmospheric models. The ability of the models to reproduce observed atmospheric perturbations generated by SPEs was evaluated, with particular respect to NO_y and ozone changes. It was found that SPE-induced ozone losses agree within 5% with the observations.

NO_x measurements by MIPAS were extensively studied by Funke et al. (2014a; 2014b). They analyzed global climatologies obtained by a decade of MIPAS observations. Contributions from EPP-induced NO_y to the total column of polar stratospheric and mesospheric NOy were found to be up to 30-40% with differences between the two hemispheres. The highest EPP-NO_y concentrations were found in the winter mesosphere. The interannual variability and hemispheric differences of NO_y produced by EPP and subsequent transport into the stratosphere during polar winters were studied. The amount of NO_y transported into the stratosphere of the northern hemisphere is typically 2-5 times smaller than in the southern hemisphere, the cause being lower descent rates and stability of the polar vortex. They show that a large fraction of the interannual variability of EPP-NO_y in the southern hemisphere can be linked to variations in geomagnetic activity.

A pronounced minimum is observed in NO_x in the mesosphere due to NO destruction (via hν and N). NO_x enhancements in the MLT region have been measured by the MIPAS, ACE-FTS, LIMS and HALOE instruments (also by SCIAMACHY, SMR and OSIRIS, but only NO) and have been modelled by Chemical Transport Models (CTMs). It is known that in the middle mesosphere and above NO_x has a lifetime of days or less, as it is destroyed by photodissociation and recombination. Since during the polar winter when sunlight duration is short, throughout the MLT lifetimes are long enough that NO_x may descent to the lower mesosphere without being photochemically destroyed. Once NO reaches the lower mesosphere, its lifetime becomes longer because of less photodissociation. Therefore in the lower mesosphere there is sufficient time for the NO_x to descend to the stratosphere, where it has a lifetime as long as a year. Once in the stratosphere, NO_x can participate in the catalytic processes controlling ozone, an important mechanism for coupling the upper part of the middle atmosphere with the lower part of it. It is generally accepted that the amount of descending NO_x is driven by the EPP level and modulated by dynamics.

Other mesospheric observations of chemical species

Metal species such as Na, Mg, Mg^+, Fe, K and Ni form layers at mesospheric altitudes. Their height distribution, seasonal variation, and short-time variability is mostly inferred from ground-based observations with resonance lidars (She et al., 2000; Fricke-Begemann et al., 2002; Gardner et al., 2005; Collins et al., 2015). Mg and Mg^+ were measured by SCIAMACHY (Scharringhausen et al., 2008, Langowski et al., 2014) and previously by the Global Ozone Monitoring Experiment (GOME) on the ERS-2 satellite. Column densities for Mg and Mg^+ were retrieved from GOME data from the years 1996 and 1997 (Correira et al., 2008). Correira et al. found seasonal and latitudinal variations in both Mg and Mg^+ concentrations, where the seasonal dependence is more pronounced at mid-latitudes.

Enhancements of mesospheric N_2O that are observed during winter at polar latitudes are correlated with NO_x intrusions from the upper atmosphere, which are related to energetic particle precipitation (Funke et al., 2008, Semeniuk et al., 2008). Funke et al. (2008) report that the inter-annual variability of N_20 in the mesosphere is correlated with observed precipitating electron fluxes.

Methane measurements by HALOE in the upper stratosphere and lower stratosphere were used by Remsberg et al. (2014) to study large-scale changes of the net transport within the middle atmosphere.

Mesospheric CO is created by photolysis of CO_2 in the MLT region and is transported downward. Due to low OH concentrations in polar night conditions, CO is conserved and is a suitable tracer for studies of wintertime polar dynamics (Lee et al., 2011).

Observations of Polar Mesospheric Clouds (PMCs)

Starting from the 1970s, polar mesospheric clouds (PMCs) have been observed with several satellite sensors which were originally designed to observe other atmospheric species. Using data from these sensors, global features of PMCs have been studied (see DeLand et al. (2006) for a review of these observations). In 2007 NASA started the Aeronomy of Ice in the Mesosphere (AIM) experiment. The AIM experiment studies Polar Mesospheric Clouds (PMCs), the ice crystal clouds that form in the Earth's mesosphere. AIM helps uncover why these clouds form and why they vary, quantifying the connection between PMCs and the meteorology of the polar mesosphere. The AIM mission seeks to create a foundation for the study of long-term change in the mesosphere and its relationship to global change.

AIM data help to validate predictive models that can reliably use past PMC changes and present trends as indicators of global change. This is achieved by measuring PMC abundances, spatial distribution, particle size distributions, gravity wave activity, dust influx to the atmosphere and precise, vertical profile measurements of temperature, H_2O, OH, CH_4, O_3, CO_2, NO, and aerosols. The complements of instruments on the AIM satellite allow these data to be obtained at many locations throughout the PMC seasons.

Further investigations using data from the Solar Backscatter Ultraviolet (SBUV) satellite instruments have been carried out to study PMCs, for example the latitudinal dependence of long-term variations (DeLand et al., 2007) and studying variations in the timing of the onset of the PMC season (Benze et al., 2012).

Notably, the question whether or not PMCs do show a significant trend that is potentially driven by anthropogenic climate change is still hotly debated (Thomas et al., 2001; von Zahn,

2003; Thomas et al., 2003a;b). While the DeLand et al. (2007) claim to find a significant increase of PMC brightness in more than 30 years of observations with the SBUV suite of instruments other authors have pointed out that this data set might potentially be strongly biased by tidal effects due to the strongly varying local time coverage of the SBUV instruments (Stevens et al., 2010; Fiedler et al., 2005).

This indicates that many open points remain to be clarified. NLCs are still believed responding clearly to even small changes in their environment. Since cooling of the upper atmosphere is expected due to enhanced greenhouse gas concentrations, an increase in mesospheric cloudiness could be one consequence of mesospheric climate change.

4.2 Linking modelled and observed mesospheric data

Exemplarily, some studies are presented in this section to demonstrate the possibilities and benefits when using these observed and modelled data sets in a uniform way and how it can help to get a better understanding of individual processes and feedbacks.

Calculations with general circulation models as well as some data sets (Offermann et al., 2004, 2010; Bremer and Berger, 2002; Berger and Lübken, 2011) indicate dynamical and thermal changes in the middle atmosphere as consequences of anthropogenic CO_2 and O_3 changes. Some models indicate that the trend seen before 1980 or the 1990s was different from the trend after that time period. Such a possibility is even supported by the observational data (Offermann et al., 2010). This is difficult to understand with anthropogenic influences, and it therefore remains to be determined as to what extent the long-term variations seen may be man-made or are part of a natural climate fluctuation. Hence, trend results are likely to be dependent on the time interval chosen for analysis, which could be one of the possible reasons for the different trend results obtained by different investigators. An attempt has also been made by us to examine the possible impact on mesospheric temperature trends which might have been caused by stratospheric ozone recovery. The answer to this question is in non-affirmative so far; there are no definite convincing signals which can be correlated with the ozone trend reversal in the stratosphere. However, it could be a potential scientific problem as the ozone recovery become faster in the coming years.

Another possible source of medium-to-long-term variability in wave propagation is the 11 year solar cycle. Ern et al. (2013) presented model simulations that suggest a small increase in planetary wave activity during solar maximum. There is also some observational evidence that gravity wave momentum fluxes vary out of phase with the solar cycle in the middle stratosphere (Ern et al., 2011); however, this finding is based on just nine years of data.

A comparison between SABER observations and the HAMMONIA model (Hamburg Model of the Neutral and Ionised Atmosphere) is presented in Dikty et al. (2010). The results show a good qualitative agreement for ozone. The amplitude of daytime variations is in both cases approximately 60% of the daytime mean. During equinox the daytime maximum ozone abundance is for both, the observations and the model, higher than during solstice, especially above 0.01 hPa (approx. 80 km). Dikty and colleagues also used the HAMMONIA output of daytime variation patterns of several other different trace gas species, e.g., water vapour and atomic oxygen, to discuss the daytime pattern in ozone. In contrast to ozone, temperature data show little daytime variations between 65 and 90 km and their amplitudes are on the order of less than 1.5%. An open point was that SABER and HAMMONIA temperatures show significant differences above 80 km.

Odin/SMR water vapour measurements in the upper mesosphere and lower thermosphere with focus on the polar latitudes in winter were presented by Lossow et al. (2009). Measurements since 2003 were compiled to provide an overview of the water vapour distribution in this altitude range. The observations showed a distinct seasonal increase of the water vapour concentration during winter at altitudes above 90 km. Above 95 km the observations exhibit the annual water vapour maximum during wintertime. Respective model data derived from Hamburg Model of the Neutral and Ionized Atmosphere (HAMMONIA) and Whole Atmosphere Community Climate Model version 3 (WACCM3) simulations showed a good accordance with the observations. Both models are general circulation models (GCMs) with coupled chemistry (i.e. CCMs). Lossow and colleagues suggested that the observed increase in water vapour during winter is mainly caused by a combination of upwelling of moister air

from lower altitudes and diffusion processes. Distinct interhemispheric differences in the winter water vapour distribution in the upper mesosphere and lower thermosphere were identified, both in observations and model results. In the Northern Hemisphere in January the Odin/SMR observations exhibit lower water vapour concentrations in the entire altitude range considered here as compared to HAMMONIA and WACCM3. Above 90 km it is usually a factor 2-3 less water vapour. HAMMONIA showed more water vapour than WACCM3 below 95 km, higher up both models showed very similar concentrations. In the Southern Hemisphere in July the observed water vapour concentrations are found between the model results almost in the entire altitude range, with HAMMONIA on the high and WACCM3 on the low side. Just at the uppermost altitudes (around 100 km) the Odin/SMR observations show lower water vapour concentrations compared to WACCM3. Above 90 km the HAMMONIA water vapour concentrations are typically a factor of 2 higher than the WACCM3 concentrations. Reasons are unclear. At 110 km the Odin/SMR exhibited a factor of 2-3 lower water vapour concentrations as the model results, similar to the observed behaviour in January in the Northern Hemisphere.

To predict future climate change in the middle atmosphere and chemistry-climate interactions, CCMs are useful tools. This requires detailed evaluation exercises (e.g. see above) demonstrating the abilities of the model systems and to demonstrate that they are able to produce robust and reliable assessments. An example of such a study is presented by Kirner et al. (2014). They performed well-defined long-term simulations with boundary conditions from the Intergovernmental Panel on Climate Change (IPCC) A1B greenhouse gas scenario and the World Meteorological Organization (WMO) Ab halogen scenario using the CCM EMAC. In a first simulation they have fixed the mixing ratios of CO_2, CH_4, and N_2O in the boundary conditions to the amounts for 2000. In four additional sensitivity simulations they have fixed the boundary conditions of only one of the species CO_2, CH_4, N_2O or ODS to year 2000. As expected, they showed that enhanced CO_2 concentrations cause the largest contributions to the radiative cooling of the middle atmosphere, followed by increasing the amount of CH_4, which also forms additional H_2O in the upper stratosphere and mesosphere. Increasing N_2O mixing ratios turned out making the smallest contributions to the cooling in the stratosphere and mesosphere.

5 Open questions

Key-points for future work and why we need long-term observations

- Determine well-quantified trends in temperature at all heights and latitudes.
- Establish understanding of those changes and the role of the major driver, the increase of CO_2, which is also the major species responsible for atmospheric cooling.
- Identification of the shrinking of the upper atmosphere which is linked to the temperature trends.
- Identification of trends in atmospheric dynamics, i.e., in atmospheric circulation and particularly in atmospheric wave activity. Atmospheric waves affect many parameters of the upper atmosphere. It is expected that trends in circulation are of a complex spatial pattern.
- The agreement between observations and models is still only qualitative for many parameters. Reducing the quantitative discrepancy between observed and simulated trends is of major importance. It will result also in better understanding of mechanisms responsible for trends.
- Trends are known mostly qualitatively, not quantitatively. Specifying and quantifying trends in various parameters and studying various finer details of trend behaviour are tasks for future research. Certainly this would require long-term mesospheric observations (in the order of 30 years, i.e. 3 solar cycles); due to the lack of such long-term observations, a combined study with model results derived from multi-decadal simulations could help to close this gap a little bit.
- The changing role of trend drivers induces spatial and particularly temporal changes of trends in various dynamical parameters and concentrations changes of chemical species. This has to be monitored and further studied.
- Another important task is to join the upper atmospheric trends with long-term changes in the stratosphere into one scenario. Similarities and differences between upper atmospheric and stratospheric trends have to be studied.

6 References

Akiyoshi, H., T. Sugita, H. Kanzawa, and N. Kawamoto, Ozone perturbations in the Arctic summer lower stratosphere as a reflection of NO_x chemistry and planetary scale wave activity, *J. Geophys. Res.*, 109, D03304, doi: 10.1029/2003JD003632, 2004.

Akmaev, R.A., Whole atmosphere modeling: Connecting terrestrial and space, *Rev. Geophys., 49*, RG4004, doi: 10.1029/2011RG000364, 2011.

Allen, M., J.I. Lunine, and Y.L. Yung, The vertical distribution of ozone in the mesosphere and lower thermosphere, *J. Geophys. Res., 89(D3)*, 4841-4872, doi: 10.1029/JD089iD03p04841, 1984.

Andersson, M.E., Verronen, P.T., Rodger, C.J., Clilverd, M.A., and Seppälä, A., Missing driver in the Sun-Earth connection from energetic electron precipitation impacts mesospheric ozone, *Nature Commun*., 5:5197, doi:10.1038/ncomms6197, 2014.

Austin, J., Shindell, D., Beagley, S. R., Brühl, C., Dameris, M., Manzini, E., Nagashima, T., Newman, P., Pawson, S., Pitari, G., Rozanov, E., Schnadt, C., and Shepherd, T. G.: Uncertainties and assessments of chemistry-climate models of the stratosphere, *Atmos. Chem. Phys.*, 3, 1-27, doi:10.5194/acp-3-1-2003, 2003.

Austin, J., and N. Butchart, Coupled chemistry-climate model simulations for the period 1980 to 2020: ozone depletion and the start of ozone recovery, *Q.J.R. Meteorol. Soc.*, 129, 3225–3249, 2003.

Austin, J., et al, Coupled chemistry climate model simulations of the solar cycle in ozone and temperature, *J. Geophys. Res.*, 113, D11306, doi:10.1029/2007JD009391, 2008.

Bailey, S. M., B. Thurairajah, C.E. Randall, L. Holt, D.E. Siskind, V.L. Harvey, K. Venkataramani, M.E. Hervig, P. Rong, and J.M. Russell III, A multi tracer analysis of thermosphere to stratosphere descent triggered by the 2013 Stratospheric Sudden Warming, *Geophys. Res. Lett., 41*, 5216-5222, doi: 10.1002/2014GL059860, 2014.

Barth, C. A., Tobiska, W. K., Siskind, D. E., Cleary, D. D, Solar-terrestrial coupling: Low-latitude thermospheric nitric oxide, *Geophysical Research Letters*, Volume 15, Issue 1, pages 92–94, doi: 10.1029/GL015i001p00092, 1988.

Barth, C. A., Nitric oxide in the lower thermosphere, *Planetary and Space Science*, 40, 315–336, 1992.

Barth, C. A., K. D. Mankoff, S. M. Bailey, and S. C. Solomon, Global observations of nitric oxide in the thermosphere, *J. Geophys. Res.*, 108, 1027, doi:10.1029/2002JA009458, A1, 2003.

Beagley, S. R., J. de Grandpré, J. N. Koshyk, N. A. McFarlane, and T. G. Shepherd, Radiative-dynamical climatology of the first generation Canadian Middle Atmosphere Model, *Atmos. Ocean*, 35, 293–331, 1997.

Beagley, S. R., Boone, C. D., Fomichev, V. I., Jin, J. J., Semeniuk, K., McConnell, J. C., and Bernath, P. F.: First multi-year occultation observations of CO_2 in the MLT by ACE satellite: observations and analysis using the extended CMAM, *Atmos. Chem. Phys.*, 10, 1133-1153, doi:10.5194/acp-10-1133-2010, 2010.

Becker, E., Sensitivity of the upper mesosphere to the Lorenz energy cycle of the troposphere, *J. Atmos. Sci., 66*, 647-666, doi: 10.1175/2008JAS2735.1, 2009.

Beig, G., Trends in the mesopause region temperature and our present understanding - An update, *Phys. Chem. Earth, 31*, 3-9, doi: 10.1016/j.pce.2005.03.007, 2006.

Beig, G., Long-term trends in the temperature of the mesosphere/lower thermosphere region: 1. Anthropogenic influences, *J. Geophys. Res., 116*, doi: 10.1029/2011JA016646, 2011.

Beig, G., et al., Review of mesospheric temperature trends, *Rev. Geophys., 41(4)*, 1015, doi: 10.1029/2002RG000121, 2003.

Beig, G. , S. Fadnavis , H. Schmidt , and G. P. Brasseur, Inter-comparison of 11-year solar cycle response in mesospheric ozone and temperature obtained by HALOE satellite data and HAMMONIA model, *J. Geophys. Res.*, 117, D00P10, doi:10.1029/2011JD015697, 2012.

Bender, S., Sinnhuber, M., von Clarmann, T., Stiller, G., Funke, B., López-Puertas, M., Urban, J., Pérot, K., Walker, K. A., and Burrows, J. P., Comparison of nitric oxide measurements in the mesosphere and lower thermosphere from ACE-FTS, MIPAS, SCIAMACHY, and SMR, *Atmos. Meas. Tech. Discuss.*, 7, 12735-12794, doi:10.5194/amtd-7-12735-2014, 2014.

Benze, S., C.E. Randall, B. Karlsson, V.L. Harvey, M.T. DeLand, G.E. Thomas, and E.P. Shettle, On the onset of polar mesospheric cloud seasons as observed by SBUV, *J. Geophys. Res.*, *117*, D07104, doi: 10.1029/2011JD017350, 2012.

Berger, U., and M. Dameris, Cooling of the upper atmosphere due to CO_2 increases: A model study, *Ann. Geophysicae, 11*, 809-819, 1993.

Berger, U., and F.-J. Lübken, Mesospheric temperature trends at midlatitudes in summer, *Geophys. Res. Lett., 38*, L22804, doi: 10.1029/2011GL049528, 2011.

Berrisford, P., Dee, D. P. K. F., Fielding, K., Fuentes, M., Kallberg, P., Kobayashi, S., and Uppala, S.. The ERA-Interim Archive. 2009.

Berrisford, P., Kållberg, P., Kobayashi, S., Dee, D., Uppala, S., Simmons, A. J., ... and Sato, H.. Atmospheric conservation properties in ERA-Interim. *Quarterly Journal of the Royal Meteorological Society*, *137*(659), 1381-1399. 2011.

Bermejo-Pantaleón, D., Funke, B., López-Puertas, M., García-Comas, M., Stiller, G. P., Clarmann, von, T., Linden, A., Grabowski, U., Höpfner, M., Kiefer, M., Glatthor, N., Kellmann, S. and Lu, G.: Global observations of thermospheric temperature and nitric oxide from MIPAS spectra at 5.3 µm, *J. Geophys. Res.*, 116(A10), A10313, 2011.

Boone, C. D., Nassar, R., Walker, K. A., Rochon, Y., McLeod, S. D., Rinsland, C. P., and Bernath, P. F.. Retrievals for the atmospheric chemistry experiment Fourier-transform spectrometer. *Applied Optics*, *44*(33), 7218-7231. 2005.

Boone, Chris D., Kaley A. Walker, and Peter F. Bernath, Version 3 Retrievals for the Atmospheric Chemistry Experiment Fourier Transform Spectrometer (ACE-FTS), The Atmospheric Chemistry Experiment ACE at 10: A Solar Occultation Anthology (Peter F. Bernath, editor, A. Deepak Publishing, Hampton, Virginia, U.S.A., 103-127, 2013.

Brasseur, G., and S. Solomon, Aeronomy of the Middle Atmosphere: Chemistry and Physics of the Stratosphere and Mesosphere, 3rd ed., 646 pp., Springer, Heidelberg, Germany, 2005.

Bremer, J., and U. Berger, Mesospheric temperature trends derived from ground-based LF phase-height observations at mid-latitudes: Comparison with model simulations, *J. Atmos. Sol. Terr. Phys., 64(7),* 805-816, doi: 10.1016/S1364-6826(02)00073-1, 2002.

Bremer, J., and D. Peters, Influence of stratospheric ozone changes on long-term trends in the meso- and lower thermosphere, *J. Atmos. Solar-Terr. Phys., 70,* 1473-1481, doi: 10.1016/j.jastp.2008.03.024, 2008.

Carleer, M. R., C. D. Boone, K. A. Walker, P. F. Bernath, K. Strong, R. J. Sica, C. E. Randall, H. Vömel, J. Kar, M. Höpfner, M. Milz, T. von Clarmann, R. Kivi, J. Valverde-Canossa, C. E. Sioris, M. R. M. Izawa, E. Dupuy, C. T. McElroy, J. R. Drummond, C. R. Nowlan, J. Zou, F. Nichitiu, S. Lossow, J. Urban, D. Murtagh, and D. G. Dufour, Validation of water vapour profiles from the Atmospheric Chemistry Experiment (ACE), *Atmos. Chem. Phys. Discuss.*, 8, 4499-4559, doi:10.5194/acpd-8-4499-2008, 2008.

Ceccherini, S., Cortesi, U., Verronen, P. T., and Kyrölä, E.: Technical Note: Continuity of MIPAS-ENVISAT operational ozone data quality from full- to reduced-spectral-resolution operation mode, *Atmos. Chem. Phys.*, 8, 2201-2212, doi:10.5194/acp-8-2201-2008, 2008.

Chandra, S., C.H. Jackman, E.L. Fleming, and J.M. Russell III, The seasonal and long term changes in mesospheric water vapor, *Geophys. Res. Lett., 24*, 639-642, doi: 10.1029/97GL00546, 1997.

Chandran, A., D.W. Rusch, S.E. Palo, G.E. Thomas, M.J. Taylor, Gravity wave observations in the summertime polar mesosphere from the Cloud Imaging and Particle Size (CIPS) experiment on the AIM spacecraft, , *J. Atmos. Solar-Terr. Phys.*, Volume 71, Issues 3–4, Pages 392-400, ISSN 1364-6826, doi:/10.1016/j.jastp.2008.09.041, 2009.

Charney, J.G., and P.G. Drazin, Propagation of planetary-scale disturbances from the lower into the upper atmosphere, *J. Geophys. Res., 66*, 83-109, 1961.

Von Clarmann, T., et al. "Retrieval of temperature, H2O, O3, HNO3, CH4, N2O, ClONO2 and ClO from MIPAS reduced resolution nominal mode limb emission measurements, Atmos." *Meas. Tech* 2.1: 159-175, 2009.

Clerbaux, C., P.-F. Coheur, D. Hurtmans, B. Barret, M. Carleer, R. Colin, K. Semeniuk, J. C. McConnell, C. Boone, and P. Bernath, Carbon monoxide distribution from the ACE-FTS solar occultation measurements, *Geophys. Res. Lett.*, 32, L16S01, doi:10.1029/2005GL022394.2005, 2005.

Clerbaux, C., M. George, S. Turquety, K.A. Walker, B. Barret, P. Bernath, C. Boone, T. Borsdorff,J.P. Cammas, V. Catoire, M. Coffey, P.-F. Coheur, M. Deeter, M. De Mazière, J. Drummond, P. Duchatelet, E. Dupuy, R. de Zafra, F. Eddounia, D.P. Edwards, L. Emmons, B. Funke, J. Gille, D.W.T. Grifï¬□th, J. Hannigan, F. Hase, M. Höpfner, N. Jones, A. Kagawa, Y. Kasai, I. Kramer, E. Le Flochmoën, N.J. Livesey, M. López-Puertas, M. Luo, E. Mahieu, D. Murtagh, P. Nédélec, A. Pazmino, H. Pumphrey, P. Ricaud, C.P. Rinsland, C. Robert, M. Schneider, C. Senten, G. Stiller, A. Strandberg, K. Strong, R. Sussmann, V. Thouret, J. Urban, A. Wiacek, CO measurements from the

ACE-FTS satellite instrument: data analysis and validation using ground-based, airborne and spaceborne observations, *Atmos. Chem. Phys*. 8, 2569-2594, 2008.

Collins, R. L., J. Li, and C. M. Martus, First lidar observation of the mesospheric nickel layer, *Geophys. Res. Lett*., 42, 665–671, doi:10.1002/2014GL062716, 2015.

Connor, B.J., D.E. Siskind, J.J. Tsou, A. Parrish, and E.E. Remsberg, Ground-based microwave observations of ozone in the upper stratosphere and mesosphere, *J. Geophys. Res., 99(D8),* 16,757-16,770, doi: 10.1029/94JD01153, 1994.

Correira, J., A. C. Aikin, J. M. Grebowsky, W. D. Pesnell, and J. P. Burrows (2008), Seasonal variations of magnesium atoms in the mesosphere-thermosphere, *Geophys. Res. Lett*., 35, L06103, doi:10.1029/2007GL033047, 2008.

Crutzen, P.J., The influence of nitrogen oxides on the atmospheric ozone content, *Quart. J.* R. *Met. Soc*., *96*, 320-325, 1970.

Damiani, A., M. Storini, M. L. Santee, and S. Wang, Variability of the nighttime OH layer and mesospheric ozone at high latitudes during northern winter: influence of meteorology, *Atmos. Chem. Phys.*, *10*(21), 10291–10303, doi:10.5194/acp-10-10291-2010, 2010.

Dee, D. P., Uppala, S. M., Simmons, A. J., Berrisford, P., Poli, P., Kobayashi, S., Andrae, U., Balmaseda, M. A., Balsamo, G., Bauer, P., Bechtold, P., Beljaars, A. C. M., van de Berg, L., Bidlot, J., Bormann, N., Delsol, C., Dragani, R., Fuentes, M., Geer, A. J., Haimberger, L., Healy, S. B., Hersbach, H., Hólm, E. V., Isaksen, L., Kållberg, P., Köhler, M., Matricardi, M., McNally, A. P., Monge-Sanz, B. M., Morcrette, J.-J., Park, B.-K., Peubey, C., de Rosnay, P., Tavolato, C., Thépaut, J.-N. and Vitart, F., The ERA-Interim reanalysis: configuration and performance of the data assimilation system. Q.J.R. Meteorol. Soc., 137: 553–597. doi: 10.1002/qj.828Waters, J. W., Froidevaux, L., Harwood, R. S., Jarnot, R. F., Pickett, H. M., Read, W. G., ... & Walch, M. J. (2006). The earth observing system microwave limb sounder (EOS MLS) on the Aura satellite. *Geoscience and Remote Sensing, IEEE Transactions on*, *44*(5), 1075-1092. 2011.

Degenstein, D. A., R. L. Gattinger, N. D. Lloyd, A. E. Bourassa, J. T. Wiensz, and E. J. Llewellyn, Observations of an extended mesospheric tertiary ozone peak, , *67*, 1395–1402, doi:10.1016/j.jastp.2005.06.019, 2005.

DeLand, M.T., E.P. Shettle, G.E. Thomas, and J.J. Olivero, A quarter-century of satellite polar mesospheric cloud observations, *J. Atmos. Solar-Terr. Phys., 68*, 9-29, 2006.

DeLand, M.T., E.P. Shettle, G.E. Thomas, and J.J. Olivero, Latitude-dependent long-term variations in polar mesospheric clouds from SBUV version 3 PMC data, *J. Geophys. Res., 112*, D10315, doi: 10.1029/2006JD007857, 2007.

DeLand, M. T., E. P. Shettle, G. E. Thomas, and J. J. Olivero, Solar backscattered ultraviolet (SBUV) observations of polar mesospheric clouds (PMCs) over two solar cycles, *J. Geophys. Res.*, 108, 8445, doi:10.1029/2002JD002398, D8, 2003.

De Mazière, M., C. Vigouroux, P.F. Bernath, P. Baron, T. Blumenstock, C. Boone, C. Brogniez, V. Catoire, M. Coffey, P. Duchatelet, D. Griffith, J. Hannigan, Y. Kasai, I. Kramer, N. Jones, E. Mahieu, G.L. Manney, C. Piccolo, C. Randall, C. Robert, C. Senten, K. Strong, J. Taylor, C. Tétard, K.A. Walker, S. Wood, Validation of ACE-FTS v2.2 methane profiles from the upper troposphere to lower mesosphere, Atmos. Chem. Phys. 8, 2421-2435, 2008.

Dikty, S., H. Schmidt, M. Weber, C. von Savigny, and M.G. Mlynczak, Daytime ozone and temperature variations in the mesosphere: a comparison between SABER observations and HAMMONIA model, *Atmos. Chem. Phys.*, *10*, 8331-8339, doi: 10.5194/acp-10-8331-2010, 2010.

Donahue, T.M., B. Guenther, and J.E. Blamont, Noctilucent clouds in daytime: Circumpolar particulate layer near the summer mesopause, *J. Atmos. Sci.*, *29*, 1205-1209, 1972.

Dowdy, A. J., R. A. Vincent, D. J. Murphy, M. Tsutsumi, D. M. Riggin, and M. J. Jarvis, The large-scale dynamics of the mesosphere–lower thermosphere during the Southern Hemisphere stratospheric warming of 2002, *Geophys. Res. Lett*., 31, L14102, doi:10.1029/2004GL020282, 2004.

Dupuy, É., et al., Strato-mesospheric measurements of carbon monoxide with the Odin Sub-Millimetre Radiometer: Retrieval and first results, *Geophys. Res. Lett.*, *31*, L20101, doi:10.1029/2004GL020558, 2004.

Dupuy, E., K.A. Walker, J. Kar, C.D. Boone, C.T. McElroy, P.F. Bernath, J.R. Drummond, R. Skelton, S.D. McLeod, R.C. Hughes, C.R. Nowlan, D.G. Dufour, J. Zou, F. Nichitiu, K. Strong, P. Baron, R.M. Bevilacqua, T. Blumenstock, G.E. Bodeker, T. Borsdorff, A.E. Bourassa, H. Bovensmann, I.S. Boyd, A. Bracher, C. Brogniez, J.P. Burrows, V. Catoire, S. Ceccherini, S. Chabrillat, T. Christensen, M.T. Coffey, U. Cortesi, J. Davies, C. De Clercq, D.A. Degenstein, M. De Mazière, P. Demoulin, J. Dodion, B. Firanski, H. Fischer, G. Forbes, L. Froidevaux, D. Fussen, P. Gerard, S. Godin-Beekmann, F. Goutail, J. Granville, D. Griffith, C.S. Haley, J.W. Hannigan, M. Höpfner, J.J. Jin, A. Jones, N.B. Jones, K. Jucks, A. Kagawa, Y. Kasai, T.E. Kerzenmacher, A. Kleinböhl, A.R. Klekociuk, I. Kramer, H. Küllmann, J. Kuttippurath, E. Kyrölä, J.-C. Lambert, N.J. Livesey, E.J. Llewellyn, N.D. Lloyd, E. Mahieu, G.L. Manney, B.T. Marshall, J.C. McConnell, M.P. McCormick, I.S. McDermid, M. McHugh, C.A. McLinden, J. Mellqvist, K. Mizutani, Y. Murayama, D.P. Murtagh, H. Oelhaf, A. Parrish, S.V. Petelina, C. Piccolo, J.-P. Pommereau, C.E. Randall, C. Robert, C. Roth, M. Schneider, C. Senten, T. Steck, A. Strandberg, K.B. Strawbridge, R. Sussmann, D.P.J. Swart, D.W. Tarasick, J.R. Taylor, C. Tétard, L.W. Thomason, A.M. Thompson, M.B. Tully, J. Urban, F. Vanhellemont, C. Vigouroux, T. von Clarmann, P. von der Gathen, C. von Savigny, J.W. Waters, J.C. Witte, M. Wolff, J.M. Zawodny, Validation of ozone measurements from the Atmospheric Chemistry Experiment (ACE), *Atmos. Chem. Phys*. 9, 287-343, 2009.

Eremenko, M. N., S. V. Petelina, A. Y. Zasetsky, B. Karlsson, C. P. Rinsland, E. J. Llewellyn, and J. J. Sloan, Shape and composition of PMC particles derived from satellite remote sensing measurements, *Geophys. Res. Lett*., 32, L16S06, doi:10.1029/2005GL023013, 2005.

Erlick, C., V. Ramaswamy, and L. M. Russell, Differing regional responses to a perturbation in solar cloud absorption in the SKYHI general circulation model, *J. Geophys. Res*., 111, D06204, doi:10.1029/2005JD006491, 2006.

Ern, M., P. Preusse, J. C. Gille, C. L. Hepplewhite, M. G. Mlynczak, J. M. Russell III, and M. Riese, Implications for atmospheric dynamics derived from global observations of gravity wave momentum flux in stratosphere and mesosphere, *J. Geophys. Res*., 116, D19107, doi:10.1029/2011JD015821, 2011.

Ern, M., C. Arras, A. Faber, K. Froehlich, C. Jacobi, S. Kalisch, M. Krebsbach, P. Preusse, T. Schmidt, J. Wickert, Observations and ray tracing of gravity waves: Implications for global modeling. In: Luebken F.-J. (ed) Climate and weather of the sun-earth system (CAWSES): highlights from a priority program, 383-408, Springer, Dordrecht, The Netherlands, doi:10.1007/978-94-007-4348-9_21, 2013.

Eyring, V., et al, Assessment of temperature, trace species, and ozone in chemistry-climate model simulations of the recent past, *J. Geophys. Res.*, 111, D22308, doi:10.1029/2006JD007327, 2006.

Fiedler, J., G. Baumgarten, and G. von Cossart, Mean diurnal variations of noctilucent clouds during 7 years of lidar observations at ALOMAR, *Ann. Geophys., 23*, 1175-1181, doi: 10.5194/angeo-23-1175-2005, 2005.

Fischer, H., J. Gille, and J.M. Russell III, Water vapor in the stratosphere - Preliminary results of the LIMS experiment aboard Nimbus 7, *Adv. Space Res., 1*, 279-281, doi: 10.1016/0273-1177(81)90404-X, 1981.

Fomichev, V. I., W. E. Ward, S. R. Beagley, C. McLandress, J. C. McConnell, N. A. McFarlane, and T. G. Shepherd, Extended Canadian Middle Atmosphere Model: Zonal-mean climatology and physical parameterizations, *J. Geophys. Res*., 107*(*D10*)*, doi:10.1029/2001JD000479, 2002.

Fricke-Begemann, C., J. Höffner, and U. von Zahn, The potassium density and temperature structure in the mesopause region (80–105 km) at a low latitude (28°N), *Geophys. Res. Lett*., 29(22), 2067, doi:10.1029/2002GL015578, 2002.

Fritts D.C., and M.J. Alexander, Gravity wave dynamics and effects in the middle atmosphere, *Rev. Geophys., 41*(1), 1003, doi:10.1029/2001RG000106, 2003.

Funke B., M. López-Puertas, T. von Clarmann, G. P. Stiller, H. Fischer, N. Glatthor, U. Grabowski, M. Höpfner, S. Kellmann, M. Kiefer, A. Linden, G. Mengistu Tsidu, M. Milz, T. Steck and D. Y. Wang, Retrieval of stratospheric NOx from 5.3 and 6.2 μm nonlocal thermodynamic equilibrium emissions measured by Michelson Interferometer for Passive Atmospheric Sounding (MIPAS) on Envisat, *J. Geophys. Res., 110*, D09302, doi: 10.1029/2004JD005225, 2005.

Funke, B., López-Puertas, M., Garcia-Comas, M., Stiller, G. P., von Clarmann, T., and Glatthor, N.: Mesospheric N_2O enhancements as observed by MIPAS on Envisat during the polar winters in 2002–2004, *Atmos. Chem. Phys*., 8, 5787-5800, doi:10.5194/acp-8-5787-2008, 2008.

Funke, B., López-Puertas, M., García-Comas, M., Stiller, G. P., von Clarmann, T., Höpfner, M., Glatthor, N., Grabowski, U., Kellmann, S., and Linden, A.: Carbon monoxide distributions from the upper troposphere to the mesosphere inferred from 4.7 μm non-local thermal equilibrium emissions measured by MIPAS on Envisat, *Atmos. Chem. Phys*., 9, 2387-2411, doi:10.5194/acp-9-2387-2009, 2009.

Funke, B., Baumgaertner, A., Calisto, M., Egorova, T., Jackman, C., Kieser, J., Krivolutsky, A., López-Puertas, M., Marsh, D., Reddmann, T., Rozanov, E., Salmi, S.-M., Sinnhuber, M., Stiller, G. P., Verronen, P. T., Versick, S., Clarmann, von, T., Vyushkova, T., Wieters, N. and Wissing, J.: Composition changes after the “Halloween” solar proton event: the High Energy Particle Precipitation in the Atmosphere (HEPPA) model versus MIPAS data intercomparison study, *Atmos. Chem. Phys*., 11(17), 9089–9139, 2011.

Funke, B., López-Puertas, M., Holt, L., Randall, C. E., Stiller, G. P. and Clarmann, von, T.: Hemispheric distributions and interannual variability of NOy produced by energetic particle precipitation in 2002–2012, *J. Geophys. Res*., 119, 1–18, doi:10.1002/2014JD022423, 2014a.

Funke, B., López-Puertas, M., Stiller, G. P. and Clarmann, von, T.: Mesospheric and stratospheric NOy produced by energetic particle precipitation during 2002–2012, *J. Geophys. Res.*, 119(7), 4429–4446, doi:10.1002/2013JD021404, 2014b.

Garcia, R.R., D.R. Marsh, D.E. Kinnison, B.A. Boville, and F. Sassi, Simulation of secular trends in the middle atmosphere, 1950-2003, *J. Geophys. Res., 112*, D09301, doi: 10.1029/2006JD007485, 2007.

García-Comas, M., Funke, B., López-Puertas, M., Bermejo-Pantaleón, D., Glatthor, N., Clarmann, von, T., Stiller, G. P., Grabowski, U., Boone, C. D., French, W. J. R., Leblanc, T., López-Gonzalez, M. J. and Schwartz, M. J.: On the quality of MIPAS kinetic temperature in the middle atmosphere, *Atmos. Chem. Phys*., 12(13), 6009–6039, doi:10.5194/acp-12-6009-2012, 2012.

García-Comas, M., Funke, B., Gardini, A., López-Puertas, M., Jurado-Navarro, A., Clarmann, von, T., Stiller, G. P., Kiefer, M., Boone, C. D., Leblanc, T., Marshall, B. T., Schwartz, M. J. and Sheese, P. E.: MIPAS temperature from the stratosphere to the lower thermosphere: Comparison of vM21 with ACE-FTS, MLS, OSIRIS, SABER, SOFIE and lidar measurements, *Atmos. Meas. Tech*., 7(11), 3633–3651, 2014.

Gardner, C. S., J. M. C. Plane, W. Pan, T. Vondra, B. J. Murray, and X. Chu, Seasonal variations of the Na and Fe layers at the South Pole and their implications for the chemistry and general circulation of the polar mesosphere, *J. Geophys. Res*., 110, D10302, doi:10.1029/2004JD005670, 2005.

de Grandpré, J., S. R. Beagley, V. I. Fomichev, E. Griffioen, J. C. McConnell, A. S. Medvedev, and T. G. Shepherd, Ozone climatology using interactive chemistry: Results from the Canadian Middle Atmosphere Model, *J. Geophys. Res.*, 105, 26,475–26,492, 2000.

Gómez-Ramírez, D., John W. C. McNabb, James M. Russell, Mark E. Hervig, Lance E. Deaver, Greg Paxton, and Peter F. Bernath, Empirical correction of thermal responses in the Solar Occultation for Ice Experiment nitric oxide measurements and initial data validation results, *Appl. Opt*. 52, 2950-2959, 2013.

Gordley, Larry L., Mark E. Hervig, Chad Fish, James M. Russell III, Scott Bailey, James Cook, Scott Hansen, Andrew Shumway, Greg Paxton, Lance Deaver, Tom Marshall, John Burton, Brian Magill, Chris Brown, Earl Thompson, John Kemp, The solar occultation for ice experiment, *J. Atmos. Solar-Terr. Phys.*, Volume 71, Issues 3–4, Pages 300-315, ISSN 1364-6826, doi:10.1016/j.jastp.2008.07.012, 2009.

Gordley, L. L., et al., Validation of nitric oxide and nitrogen dioxide measurements made by the Halogen Occultation Experiment for UARS platform, *J. Geophys. Res.,* 101*(*D6*),* 10241–10266, doi:10.1029/95JD02143, 1996.

Granier, C., Bessagnet, B., Bond, T., D'Angiola, A., Van Der Gon, H. D., Frost, G. J., ... & Van Vuuren, D. P.. Evolution of anthropogenic and biomass burning emissions of air pollutants at global and regional scales during the 1980–2010 period. *Climatic Change*, *109*(1-2), 163-190. 2011.

Haefele, A., K. Hocke, N. Kämpfer, P. Keckhut, M. Marchand, S. Bekki, B. Morel, T. Egorova, and E. Rozanov, Diurnal changes in middle atmospheric H_2O and O_3: Observations in the Alpine region and climate models, *J. Geophys. Res., 113*, D17303, doi: 10.1029/2008JD009892, 2008.

Hamilton, K., R. John Wilson, and Richard S. Hemler: Spontaneous Stratospheric QBO-like Oscillations Simulated by the GFDL SKYHI General Circulation Model. *J. Atmos. Sci.*, 58, 3271–3292, 2001.

Hamilton, K., R. John Wilson, J. D. Mahlman, and L. J. Umscheid: Climatology of the SKYHI Troposphere–Stratosphere–Mesosphere General Circulation Model. *J. Atmos. Sci.*, 52, 5–43, 1995.

Hansen, J., R. Ruedy, J. Glascoe, and M. Sato, GISS analysis of surface temperature change, *J. Geophys. Res.*, 104*(*D24*)*, 30997–31022, doi:10.1029/1999JD900835, 1999.

Hansen, J., Sato, M., Ruedy, R., Kharecha, P., Lacis, A., Miller, R., Nazarenko, L., Lo, K., Schmidt, G. A., Russell, G., Aleinov, I., Bauer, S., Baum, E., Cairns, B., Canuto, V., Chandler, M., Cheng, Y., Cohen, A., Del Genio, A., Faluvegi, G., Fleming, E., Friend, A., Hall, T., Jackman, C., Jonas, J., Kelley, M., Kiang, N. Y., Koch, D., Labow, G., Lerner, J., Menon, S., Novakov, T., Oinas, V., Perlwitz, Ja., Perlwitz, Ju., Rind, D., Romanou, A., Schmunk, R., Shindell, D., Stone, P., Sun, S., Streets, D., Tausnev, N., Thresher, D., Unger, N., Yao, M., and Zhang, S.: Dangerous human-made interference with climate: a GISS modelE study, *Atmos. Chem. Phys.*, 7, 2287-2312, doi:10.5194/acp-7-2287-2007, 2007.

Harries, J. E., J. M. Russell III, A. F. Tuck, L. L. Gordley, P. Purcell, K. Stone, R. M. Bevilacqua, M. Gunson, G. Nedoluha, and W. A. Traub, Validation of measurements of water vapor from the Halogen Occultation Experiment (HALOE), *J. Geophys. Res.*, 101*(*D6*)*, 10205–10216, doi*:*10.1029/95JD02933, 1996.

Hartogh, P., C. Jarchow, G. R. Sonnemann, and M. Grygalashvyly, On the spatiotemporal behaviour of ozone within the upper mesosphere/mesopause region under nearly polar night conditions, *J. Geophys. Res.*, 109, D18303, doi:10.1029/2004JD004576, 2004.

Hartogh, P., C. Jarchow, G. R. Sonnemann, and M. Grygalashvyly, Ozone distribution in the middle latitude mesosphere as derived from microwave measurements at Lindau (51.66°N, 10.13°E), *J. Geophys. Res. Atmos.*, *116*(D4), doi:10.1029/2010JD014393, 2011.

Hervig, M., M. McHugh, and M.E. Summers, Water vapor enhancement in the polar summer mesosphere and its relationship to polar mesospheric clouds, *Geophys. Res. Lett., 30(20)*, 2041, doi: 10.1029/2003GL018089, 2003.

Hervig, M. E., Larry L. Gordley, James M. Russell III, Scott M. Bailey, SOFIE PMC observations during the northern summer of 2007 *J. Atmos. Solar-Terr. Phys.*, Volume 71, Issues 3–4, Pages 331-339, ISSN 1364-6826, doi:10.1016/j.jastp.2008.08.010, 2009.

Hoffmann, P., M. Rapp, W. Singer, and D. Keuer, Trends of mesospheric gravity waves at northern middle latitudes during summer, *J. Geophys. Res., 116*, D00P08, doi: 10.1029/2011JD015717, 2011.

Hood, L. L., and B. E. Soukharev, Solar induced variations of odd nitrogen: Multiple regression analysis of UARS HALOE data, *Geophys. Res. Lett.*, 33, L22805, doi:10.1029/2006GL028122, 2006.

Huang, F.T., H.G. Mayr, C.A. Reber, J.M. Russell, M. Mlynczak, and J.G. Mengel, Stratospheric and mesospheric temperature variations for the quasi-biennial and semiannual (QBO and SAO) oscillations based on measurements from SABER (TIMED) and MLS (UARS), *Ann. Geophys., 24*, 2131-2149, 2006.

Huang, F.T., H.G. Mayr, C.A. Reber, J.M. Russell III, M.G. Mlynczak, and J.G. Mengel, Ozone quasi-biennial oscillations (QBO), semiannual oscillations (SAO), and correlations with temperature in the mesosphere, lower thermosphere, and stratosphere, based on measurements from SABER on TIMED and MLS on UARS, *J. Geophys. Res., 113*, A01316, doi: 10.1029/2007JA012634, 2008.

Huang, F.T., H.G. Mayr, J.M. Russell III, and M.G. Mlynczak, Ozone diurnal variations in the stratosphere and lower mesosphere, based on measurements from SABER on TIMED, *J. Geophys. Res., 115*, D24308, doi: 10.1029/2010JD014484, 2010.

Huang, F.T., H.G. Mayr, J.M. Russell III, and M.G. Mlynczak, Ozone and temperature decadal trends in the stratosphere, mesosphere and lower thermosphere, based on measurements from SABER on TIMED, *Ann. Geophys., 32*, 935-949, doi: 10.5194/angeo-32-935-2014, 2014.

Hurrell, J.W., et al., The Community Earth System Model: A framework for collaborative research, *Bull. Am. Meteorol. Soc.*, 94(9), 1339-1360, doi: 10.1175/BAMS-D-12-00121.1, 2013.

Hurst, D. F., S.J. Oltmans, H. Vömel, K.H. Rosenlof, S.M. Davis, E.A. Ray, E.G. Hall, and A.F. Jordan, Stratospheric water vapor trends over Boulder, Colorado: Analysis of the 30 year Boulder record, *J. Geophys. Res.*, 116, D02306, doi: 10.1029/2010JD015065, 2011.

Jackson, D.R., M.D. Burrage, J.E. Harries, L.J. Gray, and J.M. Russell, The semi-annual oscillation in upper stratospheric and mesospheric water vapour as observed by HALOE, *Q. J. Roy. Meteor. Soc., 124*, 2493-2515, doi: 10.1256/smsqj.55115, 1998.

Jacobi, Ch., and D. Kürschner, Long-term trends of MLT region winds over Central Europe, *Phys. Chem. Earth, 31*, 16-21, 2006.

Jégou, Fabrice, et al. "Technical Note: Validation of Odin/SMR limb observations of ozone, comparisons with OSIRIS, POAM III, ground-based and balloon-borne instruments." *Atmos. Chem. Phys.*, 8.13: 3385-3409, 2008.

Jin, J. J., Semeniuk, K., Beagley, S. R., Fomichev, V. I., Jonsson, A. I., McConnell, J. C., Urban, J., Murtagh, D., Manney, G. L., Boone, C. D., Bernath, P. F., Walker, K. A., Barret, B., Ricaud, P., and Dupuy, E.: Comparison of CMAM simulations of carbon monoxide (CO), nitrous oxide (N_2O), and methane (CH_4) with observations from Odin/SMR, ACE-FTS, and Aura/MLS, *Atmos. Chem. Phys.*, 9, 3233-3252, doi:10.5194/acp-9-3233-2009, 2009.

Jöckel, P., H. Tost, A. Pozzer, C. Brühl, J. Buchholz, L. Ganzeveld, P. Hoor, A. Kerkweg, M.G. Lawrence, R. Sander, B. Steil, G. Stiller, M. Tanarhte, D. Taraborrelli, J. van Aardenne, J. Lelieveld, The atmospheric chemistry general circulation model ECHAM5/MESSy1: consistent simulation of ozone from the surface to the mesosphere, *Atmos. Chem. Phys., 6*, 5067-5104, 2006.

Kerzenmacher, T., M.A. Wolff, K. Strong, E. Dupuy, K.A. Walker, L.K. Amekudzi, R.L. Batchelor, P.F. Bernath, G. Berthet, T. Blumenstock, C.D. Boone, K. Bramstedt, C. Brogniez, S. Brohede, J.P. Burrows, V. Catoire, J. Dodion, J.R. Drummond, D.G.

Dufour, B. Funke, D. Fussen, F. Goutail, D.W.T. Griffith, C.S. Haley, F. Hendrick, M. Höpfner, N. Huret, N. Jones, J. Kar, I. Kramer, E.J. Llewellyn, M. López-Puertas, G. Manney, C.T. McElroy, C.A. McLinden, S. Melo, S. Mikuteit, D. Murtagh, F. Nichitiu, J. Notholt, C. Nowlan, C. Piccolo, J.-P. Pommereau, C. Randall, P. Raspollini, M. Ridolfi, A. Richter, M. Schneider, O. Schrems, M. Silicani, G.P. Stiller, J. Taylor, C. Tétard, M. Toohey, F. Vanhellemont, T. Warneke, J.M. Zawodny, J. Zou, Validation of NO2 and NO from the Atmospheric Chemistry Experiment (ACE), *Atmos. Chem. Phys.*, 8, 5801-5841, 2008.

Kirner, O., R. Ruhnke, and B.-M. Sinnhuber, Chemistry-climate interactions of stratospheric and mesospheric ozone in EMAC long-term simulations with different boundary conditions for CO_2, CH_4, N_2O, and ODS, *Atmosphere-Ocean*, doi: 10.1080/07055900.2014.980718, 2014.

Koshyk, John N. and Kevin Hamilton: The Horizontal Kinetic Energy Spectrum and Spectral Budget Simulated by a High-Resolution Troposphere–Stratosphere–Mesosphere GCM. *J. Atmos. Sci.*, 58, 329–348, 2001.

Kyrölä, E., J. Tamminen, G. W. Leppelmeier, V. Sofieva, S. Hassinen, A. Seppälä, P. T. Verronen, J. L. Bertaux, A. Hauchecorne, F. Dalaudier, D. Fussen, F. Vanhellemont, O. Fanton d'Andon, G. Barrot, A. Mangin, B. Theodore, M. Guirlet, R. Koopman, L. Saavedra de Miguel, P. Snoeij, T. Fehr, Y. Meijer and R. Fraisse, Nighttime ozone profiles in the stratosphere and mesosphere by the Global Ozone Monitoring by Occultation of Stars on Envisat, *J. Geophys. Res.*, doi: 10.1029/2006JD007193, 2006.

Kyrölä, E., Tamminen, J., Sofieva, V., Bertaux, J. L., Hauchecorne, A., Dalaudier, F., Fussen, D., Vanhellemont, F., Fanton d'Andon, O., Barrot, G., Guirlet, M., Fehr, T., and Saavedra de Miguel, L.: GOMOS O_3, NO_2, and NO_3 observations in 2002–2008, *Atmos. Chem. Phys.*, 10, 7723-7738, doi:10.5194/acp-10-7723-2010, 2010.

Kyrölä, E., M. Laine, V. Sofieva, J. Tamminen, S.-M. Päivärinta, S. Tukiainen, J. Zawodny, L. Thomason, Combined SAGE II–GOMOS ozone profile data set for 1984–2011 and trend analysis of the vertical distribution of ozone, *Atmos. Chem. Phys.*, 13, 10645-10658, doi:10.5194/acp-13-10645-2013, 2013.

Lamarque, J.-F., Bond, T. C., Eyring, V., Granier, C., Heil, A., Klimont, Z., Lee, D., Liousse, C., Mieville, A., Owen, B., Schultz, M. G., Shindell, D., Smith, S. J., Stehfest, E., Van Aardenne, J., Cooper, O. R., Kainuma, M., Mahowald, N., McConnell, J. R., Naik, V., Riahi, K., and van Vuuren, D. P.: Historical (1850–2000) gridded anthropogenic and biomass burning emissions of reactive gases and aerosols: methodology and application, *Atmos. Chem. Phys.*, 10, 7017-7039, doi:10.5194/acp-10-7017-2010, 2010.

McLandress, C., W. E. Ward, V. I. Fomichev, K. Semeniuk, S. R. Beagley, N. A. McFarlane, *and* T. G. Shepherd, Large-scale dynamics of the mesosphere and lower thermosphere: An analysis using the extended Canadian Middle Atmosphere Model, *J. Geophys. Res.*, 111, *D17111*, doi:10.1029/2005JD006776, 2006.

McLandress, C., G. G. Shepherd, B. H. Solheim, M. D. Burrage, P. B. Hays, and W. R. Skinner, Combined mesosphere/thermosphere winds using WINDII and HRDI data from the Upper Atmosphere Research Satellite, *J. Geophys. Res.*, 101*(*D6*)*, 10441–10453, doi:10.1029/95JD01706, 1996.

Langowski, M., Sinnhuber, M., Aikin, A. C., von Savigny, C., and Burrows, J. P.: Retrieval algorithm for densities of mesospheric and lower thermospheric metal atom and ion species from satellite-borne limb emission signals, *Atmos. Meas. Tech.*, 7, 29-48, doi:10.5194/amt-7-29-2014, 2014.

Lee, J. N., D. L. Wu, G. L. Manney, M. J. Schwartz, A. Lambert, N. J. Livesey, K. R. Minschwaner, H. C. Pumphrey, and W. G. Read *(*2011*),* Aura Microwave Limb Sounder observations of the polar middle atmosphere: Dynamics and transport of CO and H_2O, *J. Geophys. Res.*, 116, D05110, doi:10.1029/2010JD014608.

Liu, H.-L., and R. G. Roble, A study of a self-generated stratospheric sudden warming and its mesospheric–lower thermospheric impacts using the coupled TIME-GCM/CCM3, *J. Geophys. Res.*, 107(D23), 4695, doi:10.1029/2001JD001533, 2002.

Liu, X., Jia Yue, J. Xu, L. Wang, W. Yuan, J. M. Russell III and M. E. Hervig, Gravity wave variations in the polar stratosphere and mesosphere from SOFIE/AIM temperature observations, *J. Geophys. Res. Atmos.*,119, 7368-7381, doi: 10.1002/2013JD021439, 2014.

Livesey, N. J., et al., Validation of Aura Microwave Limb Sounder O_3 and CO observations in the upper troposphere and lower stratosphere, *J. Geophys. Res*., 113, *D15S02, doi:*10.1029/2007JD008805, 2008.

López-Puertas, M., M. García-Comas, B. Funke, D. Bermejo-Pantaleón, M. Höpfner, U. Grabowski, G. P. Stiller, T. von Clarmann, and C. von Savigny, Measurements of polar mesospheric clouds in infrared emission by MIPAS/ENVISAT, *J. Geophys. Res.*, 114, D00I07, doi:10.1029/2009JD012548, 2009.

López-Puertas, M. et al., personal communication, 2012.

Lossow, S., J. Urban, J. Gumbel, P. Eriksson, and D. Murtagh, Observations of the mesospheric semi-annual oscillation (MSAO) in water vapour by Odin/SMR, *Atmos. Chem. Phys., 8*, 6527-6540, 2008.

Lossow, S., J. Urban, H. Schmidt, D.R. Marsh, J. Gumbel, P. Eriksson, and D. Murtagh, Wintertime water vapor in the polar upper mesosphere and lower thermosphere: First satellite observations by Odin submillimeter radiometer, *J. Geophys. Res., 114*, D10304, doi: 10.1029/2008JD011462, 2009.

Matthes, K., U. Langematz, L. L. Gray, K. Kodera, *and* K. Labitzke, Improved 11-year solar signal in the Freie Universität Berlin Climate Middle Atmosphere Model (FUB-CMAM), *J. Geophys. Res.*, 109, D06101, doi:10.1029/2003JD004012, 2004.

Marsh, D., A. Smith, G. Brasseur, M. Kaufmann, and K. Grossmann, The existence of a tertiary ozone maximum in the high latitude middle mesosphere, *Geophys. Res. Lett., 28*(24), 4531–4534, 2001.

Marsh, D.R., W.R. Skinner, A.R. Marshall, P.B. Hays, D.A. Ortland, and J.-H. Yee, High Resolution Doppler Imager observations of ozone in the mesosphere and lower thermosphere, *J. Geophys. Res., 107(D19)*, 4390, doi: 10.1029/2001JD001505, 2002.

Marsh, Daniel R., Michael J. Mills, Douglas E. Kinnison, Jean-Francois Lamarque, Natalia Calvo, and Lorenzo M. Polvani: Climate Change from 1850 to 2005 Simulated in CESM1(WACCM). *J. Climate*, 26, 7372–7391, 2013.

Matsuno,T, A Dynamical Model of the Stratospheric Sudden Warming. *J. Atmos. Sci*., 28, 1479–1494. doi:10.1175/1520-0469(1971)028<1479:ADMOTS>2.0.CO;2, 1971.

Mertens, C. J., Mlynczak, M. G., López-Puertas, M., Wintersteiner, P. P., Picard, R. H., Winick, J. R., ... and Russell, J. M.. Retrieval of mesospheric and lower thermospheric kinetic temperature from measurements of CO2 15 μm Earth Limb Emission under non-LTE conditions, *Geophys. Res. Lett*, *28*(7), 1391-1394. 2001.

Mertens, C. J., James M. Russell III, Martin G. Mlynczak, Chiao-Yao She, Francis J. Schmidlin, Richard A. Goldberg, Manuel López-Puertas, Peter P. Wintersteiner, Richard H. Picard, Jeremy R. Winick, Xiaojing Xu, Kinetic temperature and carbon dioxide from broadband infrared limb emission measurements taken from the TIMED/SABER instrument, *Advances in Space Research*, Volume 43, Issue 1, Pages 15-27, ISSN 0273-1177, doi:10.1016/j.asr.2008.04.017. 2009.

Mertens, C. J., et al., SABER observations of mesospheric temperatures and comparisons with falling sphere measurements taken during the 2002 summer MaCWAVE campaign, *Geophys. Res. Lett*., 31, *L03105*, doi:10.1029/2003GL018605, 2004.

Mieruch, S., Weber, M., von Savigny, C., Rozanov, A., Bovensmann, H., Burrows, J. P., Bernath, P. F., Boone, C. D., Froidevaux, L., Gordley, L. L., Mlynczak, M. G., Russell III, J. M., Thomason, L. W., Walker, K. A., and Zawodny, J. M.: Global and long-term comparison of SCIAMACHY limb ozone profiles with correlative satellite data (2002–2008), *Atmos. Meas. Tech*., 5, 771-788, doi:10.5194/amt-5-771-2012, 2012.

Milz, M., et al., Water vapor distributions measured with the Michelson Interferometer for Passive Atmospheric Sounding on board Envisat (MIPAS/Envisat), *J. Geophys. Res*., 110, D24307, doi:10.1029/2005JD005973, 2005.

Mote, P.W., K.H. Rosenlof, M.E. McIntyre, E.S. Carr, J.C. Gille, J.R. Holton, J.S. Kinnersley, H.C. Pumphrey, J.M. Russell III, and J.W. Waters, An atmospheric tape recorder: The imprint of tropical tropopause temperatures on stratospheric water vapor, *J. Geophys. Res.*, *101*, 3989-4006, doi: 10.1029/95JD03422, 1996.

Murtagh, D., Frisk, U., Merino, F., Ridal, M., Jonsson, A., Stegman, J., ... & Oikarinen, L. (2002). An overview of the Odin atmospheric mission. *Canadian Journal of Physics*, *80*(4), 309-319.

Nassar, R., P.F. Bernath, C.D. Boone, G.L. Manney, S.D. McLeod, C.P. Rinsland, R. Skelton, and K.A. Walker, ACE-FTS measurements across the edge of the winter 2004 Arctic vortex, *Geophys. Res. Lett., 32*, L15S05, doi: 10.1029/2005GL022671, 2005.

Neale, Richard B., et al. "The mean climate of the Community Atmosphere Model (CAM4) in forced SST and fully coupled experiments." *Journal of Climate* 26.14, 5150-5168, 2013.

Nedoluha, G. E., R. M. Gomez, H. Neal, A. Lambert, D. Hurst, C. Boone and G. Stiller, Validation of long-term measurements of water vapor from the midstratosphere to the mesosphere at two Network for the Detection of Atmospheric Composition Change sites, *J. Geophys. Res.*, doi: 10.1029/2012JD018900, 2013.

Nedoluha, G.E., R.M. Bevilacqua, R.M. Gomez, W.B. Waltman, B.C. Hicks, D.L. Thacker, and W.A. Matthews, Measurements of water vapor in the middle atmosphere and implications for mesospheric transport, *J. Geophys. Res., 101*, 21,183-21,194, doi: 10.1029/96JD01741, 1996.

Norton, W. A., and J. Thuburn. "The mesosphere in the extended UGAMP GCM." Gravity Wave Processes. Springer Berlin Heidelberg, 1997. 383-401.

Offermann, D., M. Donner, P. Knieling, and B. Naujokat, Middle atmosphere temperature changes and the duration of summer, *J. Atmos. Sol. Terr. Phys., 66*, 437-450, doi: 10.1016/j.jastp.2004.01.028, 2004.

Offermann, D., P. Hoffmann, P. Knieling, R. Koppmann, J. Oberheide, and W. Steinbrecht, Long-term trends and solar cycle variations of mesospheric temperature and dynamics, *J. Geophys. Res., 115*, D18127, doi: 10.1029/2009JD013363, 2010.

Orsolini, Y. J., J. Urban, D. P. Murtagh, S. Lossow, and V. Limpasuvan, Descent from the polar mesosphere and anomalously high stratopause observed in 8 years of water vapor and temperature satellite observations by the Odin Sub-Millimeter Radiometer, *J. Geophys. Res.*, 115, D12305, doi:10.1029/2009JD013501, 2010.

Pérot, K., Hauchecorne, A., Montmessin, F., Bertaux, J. L., Blanot, L., Dalaudier, F., Fussen, D. and Kyrölä, E., First climatology of polar mesospheric clouds from GOMOS/ENVISAT stellar occultation instrument. *Atmospheric Chemistry and Physics*, 10(6), 2723-2735, 2010.

Petelina, S.V., D.A. Degenstein, E.J. Llewellyn, N.D. Lloyd, C.J. Mertens, M.G. Mlynczak, and J.M. Russell III, Thermal conditions for PMC existence derived from Odin/OSIRIS and TIMED/SABER data, *Geophys. Res. Lett*., 32, L17813, doi:10.1029/2005GL023099, 2005.

Petelina, S.V., E.J. Llewellyn, D.A. Degenstein, N.D. Lloyd, Odin/OSIRIS Limb Observations of Polar Mesospheric Clouds in 2001-2003, *J. Atmos. Space Terrest. Physics*, 68, 42-55, doi:10.1016/j.jastp.2005.08.004, 2006a.

Petelina, S.V., D.A. Degenstein, E.J. Llewellyn, N.D. Lloyd, Correlation of PMC Relative Brightness and Altitudes observed by Odin/OSIRIS in the Northern Hemisphere in 2002-2003, *J. Atmos. Space Terrest. Physics*, 68, 56-64, doi:10.1016/j.jastp.2005.08.005, 2006b.

Petelina, S.V., E.J. Llewellyn, D.A. Degenstein, Properties of Polar Mesospheric Clouds measured by Odin/OSIRIS in the Northern Hemisphere in 2002-2005, *Can. J. Phys*., 85, 1143-1158, 2007.

Petelina, S. V., and A. Y. Zasetsky, Temperature of mesospheric ice retrieved from the O-H stretch band, *Geophys. Res. Lett.*, 36, L15804, doi:10.1029/2009GL038488, 2009.

Petelina, S. V., and A. Y. Zasetsky, Temperature of mesospheric ice particles simultaneously retrieved from 850 cm^{-1} libration and 3200 cm^{-1} vibration band spectra measured by ACE-FTS, *J. Geophys. Res.*, 116, D03304, doi:10.1029/2010JD015050, 2011.

Portnyagin, Y.I., E.G. Merzlyakov, T.V. Solovjova, Ch. Jacobi, D. Kürschner, A. Manson, C. Meek, Long-term trends and year-to-year variability of mid-latitude mesosphere/lower thermosphere winds, *J. Atmos. Solar-Terr. Phys., 68*, 1890-1901, doi: 10.1016/j.jastp.2006.04.004, 2006.

Pumphrey, H. C., et al., Validation of middle-atmosphere carbon monoxide retrievals from the Microwave Limb Sounder on Aura, *J. Geophys. Res.*, 112, *D24S38, doi:*10.1029/2007JD008723, 2007.

Randel, W.J., F. Wu, J.M. Russell III, A. Roche, and J.W. Waters, Seasonal cycles and QBO variations in stratospheric CH_4 and H_2O observed in UARS HALOE data, *J. Atmos. Sci.*, *55*, 163-185, 1998.

Randel, W.J., F. Wu, H. Vömel, G.E. Nedoluha, and P. Forster, Decreases in stratospheric water vapor after 2001: Links to changes in the tropical tropopause and the Brewer-Dobson circulation, *J. Geophys. Res.*, *111*, D12312, doi: 10.1029/2005JD006744, 2006.

Randel, W.J., and E. Jensen, Physical processes in the tropical tropopause layer and their roles in a changing climate, *Nature Geosci.*, *6(3)*, 169-176, doi: 10.1038/ ngeo1733, 2013.

Reber, C.A., C.E. Trevathan, R.J. McNeal, and M.R. Luther, The Upper Atmosphere Research Satellite (UARS) mission, *J. Geophys. Res.*, *98*, 10,643-10,648, 1993.

Remsberg, E.E., J.M. Russell III, L.L. Gordley, J.C. Gille, and P.L. Bailey, Implications of the stratospheric water vapor distribution as determined from the Nimbus 7 LIMS experiment, *J. Atmos. Sci.*, *41*, 2934-2948, 1984.

Remsberg, E.E., On the observed changes in upper stratospheric and mesospheric temperatures from UARS HALOE, *Ann. Geophys.*, *26*, 1-11, 2008a.

Remsberg, E. E., B. T. Marshall, M. Garcia-Comas, D. Krueger, G. S. Lingenfelser, J. Martin-Torres5, M. G. Mlynczak, J. M. Russell III, A. K. Smith, Y. Zhao, C. Brown, L. L. Gordley, M. J. Lopez-Gonzalez, M. Lopez-Puertas, C.-Y. She, M. J. Taylor and R. E. Thompson, Assessment of the quality of the Version 1.07 temperature-versus-pressure profiles of the middle atmosphere from TIMED/SABER, *J. Geophys. Res.*,113, D17101, doi: 10.1029/2008JD010013, 2008b.

Remsberg, E.E., Trends and solar cycle effects in temperature versus altitude from the Halogen Occultation Experiment for the mesosphere and upper stratosphere, *J. Geophys. Res.*, *114*, D12303, doi: 10.1029/2009JD011897, 2009.

Remsberg, E. E.: Methane as a diagnostic tracer of changes in the net circulation of the middle atmosphere, *Atmos. Chem. Phys. Discuss*., 14, 24183-24220, doi:10.5194/acpd-14-24183-2014, 2014.

Ricaud, P., J. de la Noë, B.J. Connor, L. Froidevaux, J.W. Waters, R.S. Harwood, I.A. MacKenzie, and G.E. Peckham, Diurnal variability of mesospheric ozone as measured by the UARS Microwave Limb Sounder Instrument: Theoretical and ground-based validations, *J. Geophys. Res.*, *101(D6)*, 10,077-10,089, doi:10.1029/95JD02841, 1996.

Rind, D., J. Lerner, J. Jonas, and C. McLinden, Effects of resolution and model physics on tracer transports in the NASA Goddard Institute for Space Studies general circulation models, *J. Geophys. Res.*, 112, D09315, doi:10.1029/2006JD007476, 2007.

Rind, D., R. Suozzo, N. K. Balachandran, A. Lacis, and G. Russell: The GISS Global Climate-Middle Atmosphere Model. Part I: Model Structure and Climatology. *J. Atmos. Sci*., 45, 329–370, 1988.

Roble, R. G. and E. C. Ridley, A thermosphere-ionosphere-mesosphere-electrodynamics general circulation model (time-GCM): Equinox solar cycle minimum simulations (30–500 km), *Geophys. Res. Lett.*, Volume 21, Issue 6, pages 417–420, 1994.

Roeckner, E., R. Brokopf, M. Esch, M. Giorgetta, S. Hagemann, L. Kornblueh, E. Manzini, U. Schlese, and U. Schulzweida, Sensitivity of simulated climate to horizontal and vertical resolution in the ECHAM5 atmosphere model, *J. Climate*, *19*, 3771-3791, 2006.

Rohen G. J., C. v. Savigny, J. W. Kaiser, E. J. Llewellyn, L. Froidevaux, M. López-Puertas, T. Steck, M. Palm, H. Winkler, M. Sinnhuber, H. Bovensmann, and J. P. Burrows, Ozone profile retrieval from limb scatter measurements in the HARTLEY bands: further retrieval details and profile comparisons, *Atmos. Chem. Phys.*, 8, 2509-2517, doi:10.5194/acp-8-2509-2008, 2008.

Russell III, James M., Scott M. Bailey, Larry L. Gordley, David W. Rusch, Mihály Horányi, Mark E. Hervig, Gary E. Thomas, Cora E. Randall, David E. Siskind, Michael H. Stevens, Michael E. Summers, Michael J. Taylor, Christoph R. Englert, Patrick J. Espy, William E. McClintock, Aimee W. Merkel, The Aeronomy of Ice in the Mesosphere (AIM) mission: Overview and early science results, *Journal of Atmospheric and Solar-Terrestrial Physics*, Volume 71, Issues 3–4, Pages 289-299, ISSN 1364-6826, doi: 10.1016/j.jastp.2008.08.011, 2009.

von Savigny, C., A. Kokhanovsky, H. Bovensmann, K.-U. Eichmann, J. Kaiser, S. Noël, A.V. Rozanov, J. Skupin, J.P. Burrows, NLC detection and particle size determination: first results from SCIAMACHY on ENVISAT, Advances in Space Research, Volume 34, Issue 4, Pages 851-856, ISSN 0273-1177, doi:10.1016/j.asr.2003.05.050, 2004.

von Savigny, C., S.V. Petelina, B. Karlsson, E.J. Llewellyn, D.A. Degenstein, N.D. Lloyd, and J.P. Burrows, Vertical variation of NLC particle sizes retrieved from Odin/OSIRIS limb scattering observations, *Geophys. Res. Lett.*., 32, #7, L07806, doi:10.1029/2004GL021982, 2005.

Scharringhausen, M., Aikin, A. C., Burrows, J. P., and Sinnhuber, M., Space-borne measurements of mesospheric magnesium species – a retrieval algorithm and preliminary profiles, Atmos. Chem. Phys., 8, 1963-1983, doi:10.5194/acp-8-1963-2008, 2008.

Schmidt, H., G.P. Brasseur, M. Charron, E. Manzini, M.A. Giorgetta, T. Diehl, V.I. Fomichev, D. Kinnison, D. Marsh, and S. Walters, The HAMMONIA chemistry climate model: Sensitivity of the mesopause region to the 11-year solar cycle and CO_2 doubling, *J. Climate, 16(19)*, 3903-3931, 2006.

Schwartz, M. J., A. Lambert, G. L. Manney, W. G. Read, N. J. Livesey, L. Froidevaux, C. O. Ao, P. F. Bernath, C. D. Boone, R. E. Cofield, W. H. Daffer, B. J. Drouin, E. J. Fetzer, R. A. Fuller, R. F. Jarnot, J. H. Jiang, Y. B. Jiang, B. W. Knosp, K. Krüger, J.-L. F. Li, M. G. Mlynczak, S. Pawson, J. M. Russell III, M. L. Santee, W. V. Snyder, P. C. Stek, R. P. Thurstans, A. M. Tompkins, P. A. Wagner, K. A. Walker, J. W. Waters and D. L. Wu, Validation of the Aura Microwave Limb Sounder temperature and geopotential height measurements, *J. Geophys. Res.*, 113, D15S11, doi: 10.1029/2007JD008783, 2008.

Seele, C., and P. Hartogh, Water vapor of the polar middle atmosphere: Annual variation and summer mesosphere conditions as observed by ground-based microwave spectroscopy, *Geophys. Res. Lett., 26*, 1517-1520, doi: 10.1029/1999GL900315, 1999.

Semeniuk, K., J. C. McConnell, J. J. Jin, J. R. Jarosz, C. D. Boone, and P. F. Bernath, N_2O production by high energy auroral electron precipitation, *J. Geophys. Res.*, 113, D16302, doi:10.1029/2007JD009690, 2008.

Seppälä, A., Verronen, P.T., Kyrölä, E., Hassinen, S., Backman, L., Hauchecorne, A., Bertaux, J.L., and Fussen, D., Solar Proton Events of October-November 2003: Ozone depletion in the Northern hemisphere polar winter as seen by GOMOS/Envisat, *Geophys. Res. Lett.*, 31, L19107, doi:10.1029/2004GL021042, 2004.

Seppälä, A., P. T. Verronen, V. F. Sofieva, J. Tamminen, E. Kyrölä, C. J. Rodger, and M. A. Clilverd, Destruction of the Tertiary Ozone Maximum During a Solar Proton Event, *Geophys. Res. Lett*., 33, L07804, doi:10.1029/2005GL025571, 2006.

Seppälä, A., P. T. Verronen, M. A. Clilverd, C. E. Randall, J. Tamminen, V. Sofieva, L. Backman, and E. Kyrölä, Arctic and Antarctic polar winter NO_x and energetic particle precipitation in 2002–2006, *Geophys. Res. Lett*., 34, *L12810*, doi:10.1029/2007GL029733, 2007.

Shapiro, A. V., Rozanov, E., Shapiro, A. I., Wang, S., Egorova, T., Schmutz, W., and Peter, Th.: Signature of the 27-day solar rotation cycle in mesospheric OH and H_2O observed by the Aura Microwave Limb Sounder, *Atmos. Chem. Phys*., 12, 3181-3188, doi:10.5194/acp-12-3181-2012, 2012.

Shindell, Drew T., David Rind, and Patrick Lonergan: Climate Change and the Middle Atmosphere. Part IV: Ozone Response to Doubled CO2. *J. Climate*, 11, 895–918. doi: 10.1175/1520-0442, 1998.

She, C. Y., Chen, S., Hu, Z., Sherman, J., Vance, J. D., Vasoli, V., and Krueger, D. A., Eight-year climatology of nocturnal temperature and sodium density in the mesopause region (80 to 105 km) over Fort Collins, Co (41° N, 105° W). *Geophys. Res. Lett*., 27(20), 3289-3292, 2000.

Sheese, P. E., R. L. Gattinger, E. J. Llewellyn, C. D. Boone and K. Strong, Nighttime nitric oxide densities in the Southern Hemisphere mesosphere–lower thermosphere, *Geophys. Res. Lett., 38(15)*, L15812, doi: 10.1029/2011GL048054, 2011.

Sheese, P. E., Strong, K., Llewellyn, E. J., Gattinger, R. L., Russell III, J. M., Boone, C. D., Hervig, M. E., Sica, R. J., and Bandoro, J.: Assessment of the quality of OSIRIS mesospheric temperatures using satellite and ground-based measurements, *Atmos. Meas. Tech.*, 5, 2993-3006, doi:10.5194/amt-5-2993-2012, 2012.

Shepherd, G. G., et al., WINDII, the wind imaging interferometer on the Upper Atmosphere Research Satellite, *J. Geophys. Res*., 98*(*D6*)*, 10725–10750, doi:10.1029/93JD00227, 1993.

Shibata, K., and M. Deushi, Partitioning between resolved wave forcing and unresolved gravity wave forcing to the quasi-biennial oscillation as revealed with a coupled chemistry-climate model, *Geophys. Res. Lett.*, 32, L12820, doi:10.1029/2005GL022885, 2005.

Sica, R.J., M.R.M. Izawa, K.A. Walker, C. Boone, S.V. Petelina, P.S. Argall, P. Bernath, G. B. Burns, V. Catoire, R.L. Collins, W.H. Daffer, C. De Clercq, Z.Y. Fan, B.J. Firanski, W.J.R. French, P. Gerard, M. Gerding, J. Granville, J.L. Innis, P. Keckhut, T. Kerzenmacher, A.R. Klekociuk, E. Kyrö, J.C. Lambert, E.J. Llewellyn, G.L. Manney, I.S. McDermid, K. Mizutani, Y. Murayama, C. Piccolo, P. Raspollini, M. Ridolfi, C. Robert, W. Steinbrecht, K.B. Strawbridge, K. Strong, R. Stübi, B. Thurairajah, Validation of the Atmospheric Chemistry Experiment (ACE) version 2.2 temperature using ground based and space-borne measurements, *Atmos. Chem. Phys*. 8, 35-62, 2008.

Sinnhuber, M., J.P. Burrows, M.P. Chipperfield, C.H. Jackman, M.-B. Kallenrode, K.F. Künzi, and M. Quack, A model study of the impact of magnetic field structure on atmospheric composition during solar proton events, *Geophys. Res. Lett., 30(15)*, 1818, doi: 10.1029/2003GL017265, 2003.

Siskind, D. E., L. Coy, and P. Espy, Observations of stratospheric warmings and mesospheric coolings by the TIMED SABER instrument, *Geophys. Res. Lett.*, 32, *L09804*, doi:10.1029/2005GL022399, 2005.

Siskind, D. E., S. D. Eckermann, J. P. McCormack, L. Coy, K. W. Hoppel, and N. L. Baker, Case studies of the mesospheric response to recent minor, major, and extended stratospheric warmings, J. *Geophys. Res.*, 115, D00N03, doi:10.1029/2010JD014114, 2010.

Smith, A.K., D.R. Marsh, J.M. Russell III, M.G. Mlynczak, F.J. Martin-Torres, and E. Kyrölä, Satellite observations of high nighttime ozone at the equatorial mesopause, *J. Geophys. Res.*, *113*, D17312, doi: 10.1029/2008JD010066, 2008.

Smith, A. K., M. Lopez-Puertas, M. Garcia-Comas, and S. Tukiainen (2009), SABER observations of mesospheric ozone during NH late winter 2002-2009, *Geophys. Res. Lett.*, *36*(23), L23804, doi:10.1029/2009GL040942.

Smith, A. K., Garcia, R. R., Marsh, D. R. and Richter, J. H.: WACCM simulations of the mean circulation and trace species transport in the winter mesosphere, *J. Geophys. Res.*, 116(D20), D20115, doi:10.1029/2011JD016083, 2011.

Smith, A.K., et al., Satellite observations of ozone in the upper mesosphere, *J. Geophys. Res. Atmos.*, *118*, 5803-5821, doi: 10.1002/jgrd.50445, 2013.

Smith, A. K., M. López-Puertas, B. Funke, M. García-Comas, M. G. Mlynczak, and L. A. Holt, Nighttime ozone variability in the high latitude winter mesosphere, *J. Geophys. Res. Atmos.*, 119, 13,547–13,564, doi:10.1002/2014JD021987, 2015.

Sofieva, V. F. et al., Spatio-temporal observations of the tertiary ozone maximum, *Atmos. Chem. Phys.*, *9*(13), 4439–4445, 2009.

Stevens, M.H., et al., Tidally induced variations of polar mesospheric cloud altitudes and ice water content using a data assimilation system, *J. Geophys. Res.*, *115*, D18209, doi: 10.1029/2009JD013225, 2010.

Struthers, H., K. Kreher, J. Austin, R. Schofield, G. Bodeker, P. Johnston, H. Shiona, and A. Thomas, Changes in the rate of increase of NO_2 as predicted by a three-dimensional coupled chemistry-climate model, *Atmos. Chem. Phys.*, 4, 2227–2239, 2004.

Summers, M.E., R.R. Conway, D.E. Siskind, M.H. Stevens, D. Offermann, M. Riese, P. Preusse, D.F. Strobel, and J.M. Russell III, Implications of satellite OH observations for middle atmospheric H_2O and ozone, *Science, 277*, 1967-1970, 1997.

Summers, M.E., L.L. Gordley, and M.J. McHugh, Discovery of a water vapor layer in the Arctic summer mesosphere: Implications for polar mesospheric clouds, *Geophys. Res. Lett., 28*, 3601-3604, doi: 10.1029/2001GL013217, 2001.

Tamminen, J., E. Kyrölä, V. F. Sofieva, M. Laine, J.-L. Bertaux, A. Hauchecorne, F. Dalaudier, D. Fussen, F. Vanhellemont, O. Fanton-d'Andon, G. Barrot, A. Mangin, M. Guirlet, L. Blanot, T. Fehr, L. Saavedra de Miguel, and R. Fraisse. GOMOS data characterisation and error estimation. *Atmos. Chem. Phys*., 10, 9505-9519, 2010, doi: 10.5194/acp-10-9505-2010, 2010.

Taylor, F.W., J.J. Barnett, I. Colbeck, R.L. Jones, C.D. Rodgers, M.J. Wale, and E.J. Williamson, Performance and early results from the Stratospheric and Mesospheric

Sounder (SAMS) on Nimbus 7, *Adv. Space Res., 1*, 261-265, doi: 10.1016/0273-1177(81)90068-5, 1981.

Thomas, G.E., Are noctilucent clouds harbingers of global change in the middle atmosphere? *Adv. Space Res., 32*, 1737-1746, doi: 10.1016/0273-1177(03)00674-4, 2003a.

Thomas, G.E., and J.J. Olivero, Noctilucent clouds as possible indicators of global change in the mesosphere, *Adv. Space Res., 28*, 937-946, 2001.

Thomas, G.E., J.J. Olivero, M. DeLand, E.P. Shettle, A response to the article by U. von Zahn. ‘‘Are noctilucent clouds truly a miner’s canary of global change?’’, *EOS, Transactions-American Geophysical Union, 84 (36)*, 352-353, 2003b.

Thomason, L.W., S.P. Burton, N. Iyer, J.M. Zawodny, and J. Anderson, A revised water vapor product for the Stratospheric Aerosol and Gas Experiment (SAGE) II version 6.2 data set, *J. Geophys. Res., 109*, D06312, doi: 10.1029/2003JD004465, 2004.

Thornton, H.E., D.R. Jackson, S. Bekki, N. Bormann, Q. Errera, A.J. Geer, W.A. Lahoz, and S. Rharmili, The ASSET intercomparison of stratosphere and lower mesosphere humidity analyses, *Atmos. Chem. Phys., 9*, 995-1016, 2009.

Urban, J., et al., Odin/SMR limb observations of stratospheric trace gases: Level 2 processing of ClO, N_2O, HNO_3, and O_3, *J. Geophys. Res.*, 110, D14307, doi:10.1029/2004JD005741, 2005.

Urban, J., et al., Global observations of middle atmospheric water vapour by the Odin satellite: An overview, *Planet. Space Sci., 55*, 1093- 1102, doi: 10.1016/j.pss.2006.11.021, 2007.

Urban, J., S. Lossow, G. Stiller, and W. Read, Another drop in water vapor, *Eos, Vol. 95, No. 27*, 245-252 , 2014.

Vaughan, G., Mesospheric ozone - Theory and observation, *Q. J. R. Meteorol. Soc., 110*, 239-260, 1984.

Verronen, P. T., E. Kyrölä, J. Tamminen, B. Funke, S. Gil-López, M. Kaufmann, M. López-Puertas, T.v. Clarmann, G. Stiller, U. Grabowski, M. Höpfner, A comparison of night-time GOMOS and MIPAS ozone profiles in the stratosphere and mesosphere, *Advances in Space Research*, Volume 36, Issue 5, Pages 958-966, ISSN 0273-1177, doi:10.1016/j.asr.2005.04.073, 2005.

Verronen, P.T., Seppälä, A., Kyrölä, E., Tamminen, J., Pickett, H.M., and Turunen, E., Production of Odd Hydrogen in the Mesosphere During the January 2005 Solar Proton Event, *Geophys. Res. Lett.*, 33, L24811, doi:10.1029/2006GL028115, 2006.

Verronen, P. T., M. E. Andersson, C. J. Rodger, M. A. Clilverd, S. Wang, and E. Turunen, Comparison of modeled and observed effects of radiation belt electron precipitation on mesospheric hydroxyl and ozone, *J. Geophys. Res. Atmos.*, *118*(19), 11,411–419,428, doi:10.1002/jgrd.50845, 2013.

Walterscheid, R. L., G. G. Sivjee, and R. G. Roble, Mesospheric and lower thermospheric manifestations of a stratospheric warming event over Eureka, Canada (80°N), *Geophys. Res. Lett.*, 27(18), 2897–2900, doi:10.1029/2000GL003768, 2000.

Wang, H. J., D. M. Cunnold, L. W. Thomason, J. M. Zawodny, G. E. Bodeke. Assessment of SAGE version 6.1 ozone data quality. *J. Geophys. Res. 107*, doi: 10.1029/2002JD002418, 2002.

Waters, J. W., Froidevaux, L., Harwood, R. S., Jarnot, R. F., Pickett, H. M., Read, W. G., ... and Walch, M. J.. The earth observing system microwave limb sounder (EOS MLS) on the Aura satellite. *Geoscience and Remote Sensing, IEEE Transactions on*, *44*(5), 1075-1092, 2006.

Waymark, C., K.A. Walker, C.D. Boone, and P.F. Bernath. ACE-FTS version 3.0 data set: validation and data processing update. *Ann. Geophys*., 56:Fast Track-1, DOI: 10.4401/ag-6339 2013.

Whiteway, J. A., and A. I. Carswell: Rayleigh Lidar Observations of Thermal Structure and Gravity Wave Activity in the High Arctic during a Stratospheric Warming. *J. Atmos. Sci*., 51, 3122–3136. doi:10.1175/1520-0469(1994)051<3122:RLOOTS>2.0.CO;2, 1994.

Wrotny, J. E., Russell III, J. M., Interhemispheric differences in polar mesospheric clouds observed by the HALOE instrument, *Journal of Atmospheric and Solar-Terrestrial Physics*, Volume 68, Issue 12, Pages 1352-1369, ISSN 1364-6826, doi:10.1016/j.jastp.2006.05.014, 2006.

von Zahn, U., Are noctilucent clouds truly a ‘‘miner’s canary’’ of global change? *EOS, Transactions-American Geophysical Union*, 84 (28), 261-268, 2003.